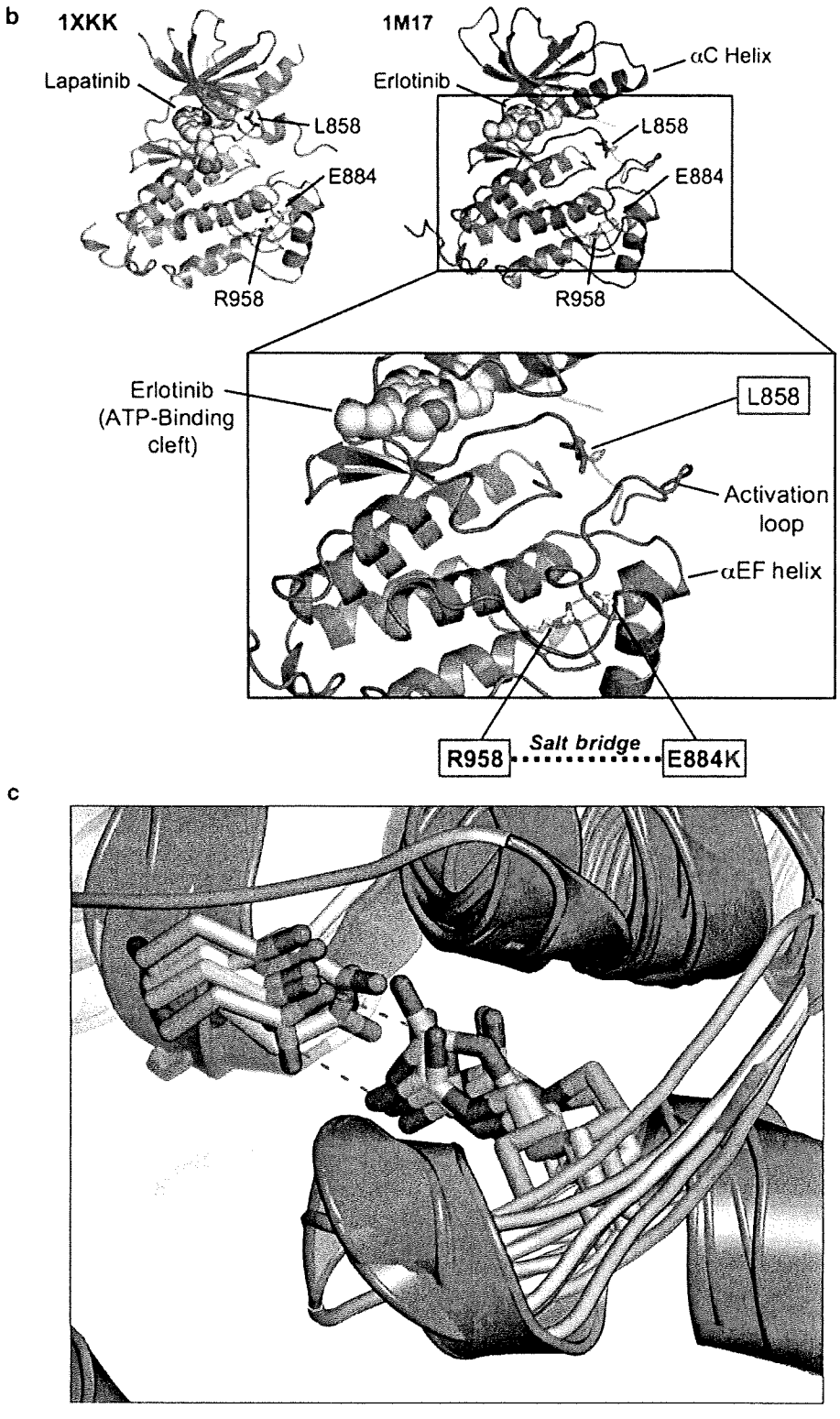

Figure 4 Continued.

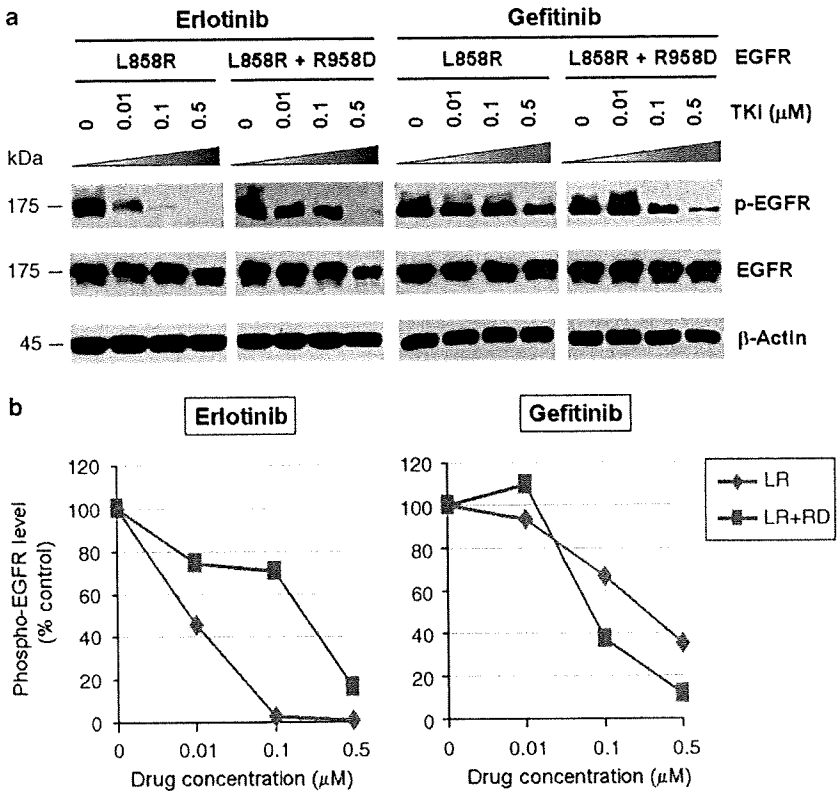

Figure 5 Disruption of the conserved Glu(E)884–Arg(R)958 salt bridge by a R958D substitution differentially altered L858R mutant receptor sensitivity to epidermal growth factor receptor (EGFR) inhibitors. (**a**) Stable COS-7 transfects expressing the sensitizing L858R and double-mutant L858R + R958D variants of EGFR were cultured in 0.5% bovine serum albumin-containing serum-free media for 16 h, and then incubated with increasing concentrations of either erlotinib or gefitinib, in the presence of EGF stimulation (100 ng/ml). Whole-cell lysates were extracted for SDS–polyacrylamide gel electrophoresis and immunoblotted using antibodies against the followings: p-EGFR (Y1068), EGFR and β-actin. R958D mutation modulated the effect of L858R on inhibitor sensitivity resulting in desensitization of the mutant receptor to erlotinib inhibition but modestly enhanced sensitivity to gefitinib inhibition. (**b**) Densitometric quantitation of the p-EGFR (Y1068) levels showing that R958D mutation differentially altered L858R mutant receptor sensitivity to erlotinib (more resistant) and gefitinib (more sensitive). Densitometric scanning of the immunoblot signals shown in (**a**) was performed using NIH ImageJ software program, with normalization to total EGFR expression levels.

2008). Stable COS-7 transfectant cells expressing similar levels of wild type and E1271K-*MET* were used in this experiment using the two reversible preclinical MET inhibitors SU11274 (Ma *et al.*, 2005a) and PHA665752 (Ma *et al.*, 2005a, b). We did not find any significant modulation of sensitivity to SU11274 inhibition in the E1271K-MET cells (Figure 6b). On the other hand, the E1271K mutation of MET enhanced the sensitivity of inhibition by PHA665752 in the phosphorylation of the mutant MET at its major autophosphorylation sites (pY1234/1235) (equivalent to pY1252/1253 phosphosites as in the full-length *MET* transcript, with a difference of 18 amino acids in the exon 10 with the common alternatively spliced variant) in the kinase domain, and its downstream signaling proteins AKT and ERK1/2 (Figure 6b). Hence, disrupting the MET kinase salt bridge by the E1271K mutation also differentially alters sensitivity to MET kinase inhibitors in an inhibitor-specific manner.

Mutations at the conserved Glu(E)–Arg(R) ion pair in the human kinome

As the E884K somatic mutation was originally identified in a never-smoker woman of Japanese descent, we performed mutational screening for the presence of mutation at the E884 and R958 residues of *EGFR* among a cohort of 67 lung tumor genomic DNA specimens from Japanese non-small-cell lung cancer patients (including 66 transbronchial biopsies and 1 surgical specimen). Nonsynonymous mutations were not present in either residue location in this patient cohort. On the basis of our results suggesting the conserved structure and function of the Glu(E)–Arg(R) ion pair in EGFR and among other kinases in the kinome, we hypothesized that there would be other cancer-associated mutations at the conserved ion pair within the human kinome in kinases other than EGFR. Here, we performed bioinformatics survey of the updated Catalog of Somatic Mutations In Cancer (COSMIC) database (http://www.sanger.ac.uk/genetics/CGP/cosmic/) containing

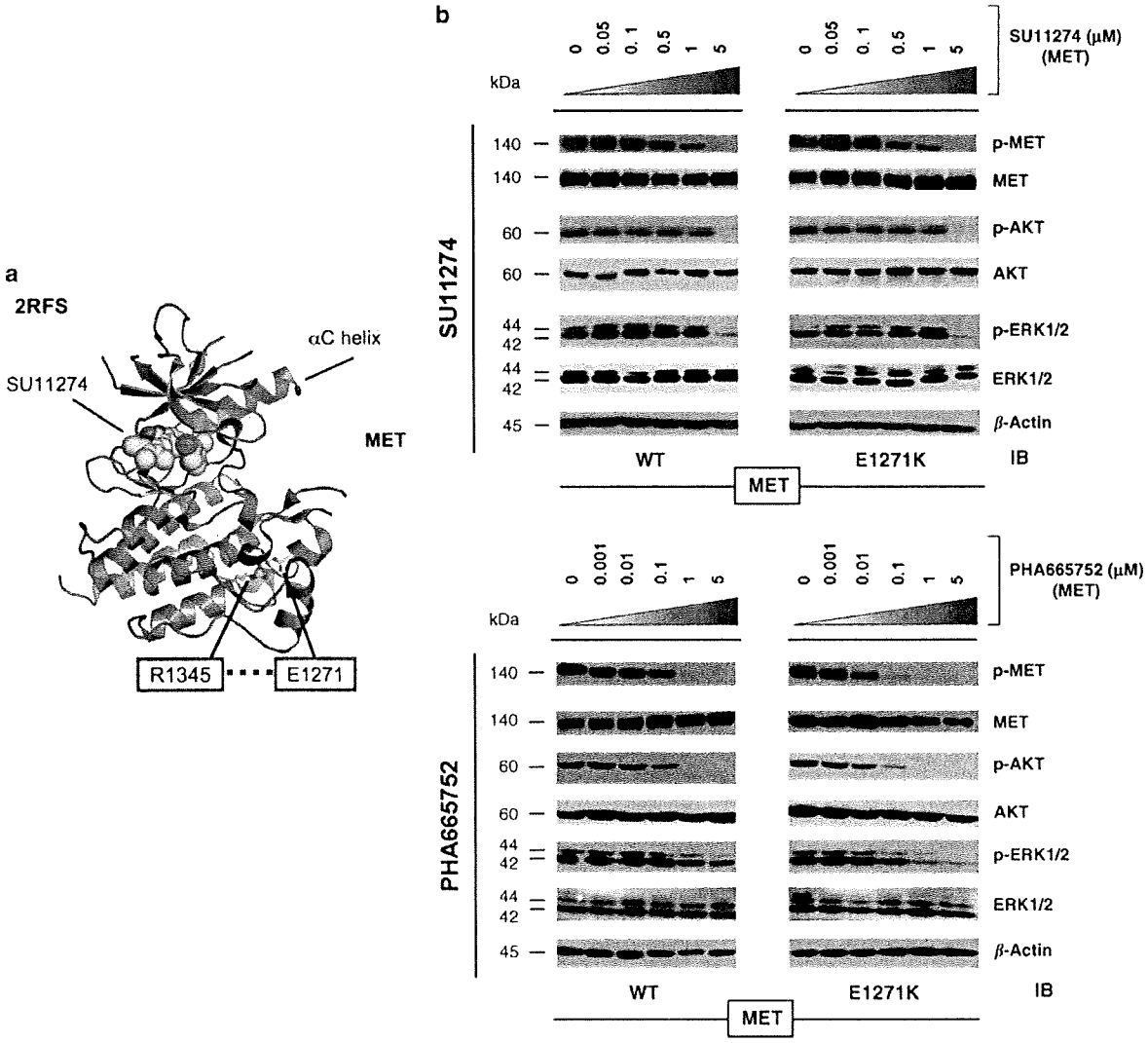

Figure 6 Mutational disruption of the conserved E1271–R1345 ion pair in MET kinase salt bridge causes inhibitor-specific modulation of sensitivity to SU11274 (unchanged) and PHA665752 (more sensitive). (**a**) MET kinase domain crystal structure (PDB accession code: 2RFS) (Bellon *et al.*, 2008) highlighting the salt bridge between E1271 and R1345. Crystal structure solved in complex with SU11274 is shown. The conserved Glu–Arg ion pair is shown in stick format, with oxygen atoms colored red, nitrogen atoms colored blue and carbon atoms colored yellow. This figure was prepared using the program PYMOL (www.pymol.org). (**b**) Stable COS-7 transfects expressing E1271K mutant *MET* were cultured in 0.5% bovine serum albumin-containing serum-free media for 16 h, then incubated with increasing concentrations of the MET inhibitors SU11274 (top) and PHA665752 (bottom) as indicated, in the presence of HGF stimulation (50 ng/ml). Whole-cell lysates were extracted for immunoblotting using antibodies against p-MET (Y1234/Y1235), MET, p-AKT, AKT, p-ERK1/2, ERK1/2 and β-actin. Wild-type *MET*-expressing COS-7 transfectant cells were included as control. E1271K mutation of MET increased the sensitivity of MET kinase phosphorylation inhibition by PHA665752.

somatic mutations identified in kinases among human cancers (Figure 7). We have conducted a complete and comprehensive survey throughout the entire human kinome for mutations identified at the conserved Glu(E)–Arg(R) ion pair in COSMIC. We also documented here the hits identifying mutations clustered in the vicinity of the ion pair, 30 amino acids proximal or distal to the Glu(E) or Arg(R). Interestingly, several kinases within the kinome were found to have mutations occurred at the Glu(E) residue, homologous to the E884–EGFR residue. These include KIT (E839K), RET (E921K), STK11/LKB1 (E223*). These are all known cancer-associated kinases that have dysregulated signaling in various human cancers, including GIST and hematological malignancies (KIT), papillary thyroid cancer (multiple endocrine neoplasm syndrome type 2) (RET) and lung cancer (RET, LKB1).

Discussion

In the era of molecularly targeted therapeutics in cancer therapy, the impact of cancer-associated mutations on kinase inhibitor sensitivity-resistance has increasingly

A[a]

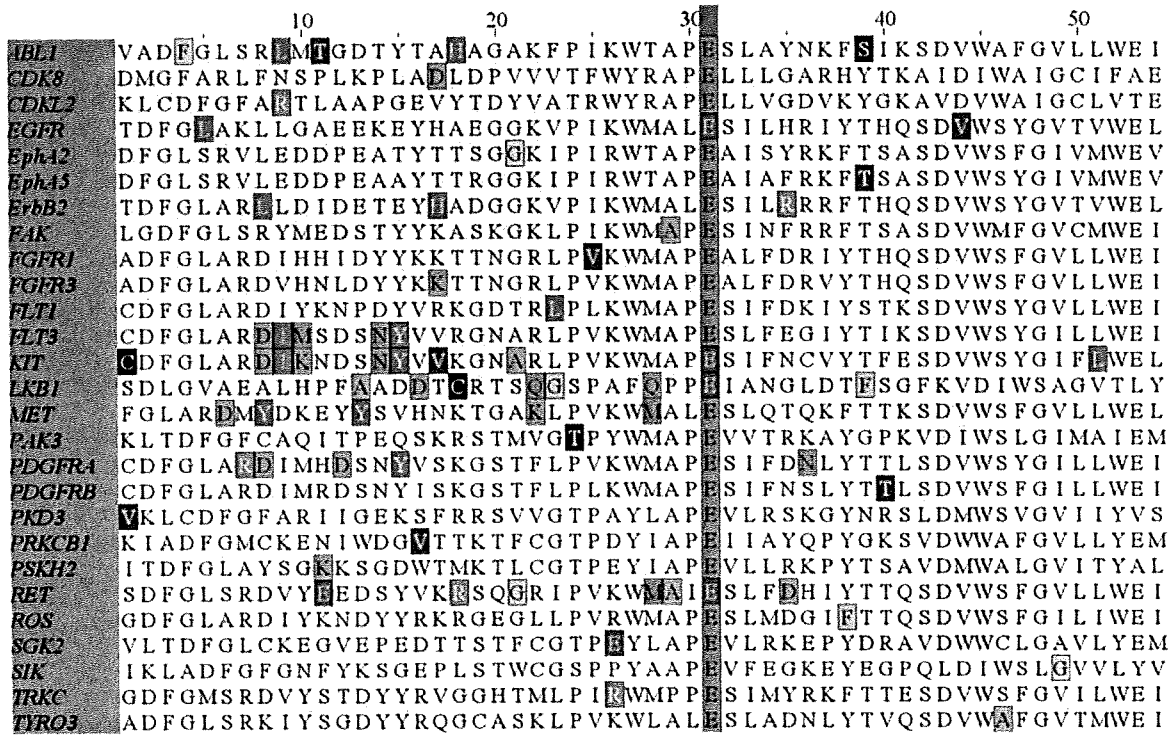

b

GENES	Mutations
ABL1:	F382L, L387M, T389A, H396P, H396R, S417Y
CDK8:	D189N
CDKL2:	R149Q
EGFR:	L858R, ***E884K***, V897I
EPHA2:	G777S
EPHA5:	T856I
ERBB2:	L869Q, H878Y, R896C
FAK:	***A612V***
FGFR1:	V664L
FGFR3:	K650E, K650M, K650Q, K650T
FLT1:	L1061V
FLT3:	D835E, D835F, D835H, D835N, D835V, D835Y, I836F, I836M, I836S, M837P, N841H, N841K, Y842C
KIT:	C809G, C809R, A814S, A814T, D816A, D816E, D816F, D816G, D816H, D816I, D816N, D816V, D816Y, I817V, K818R, D820E, D820G, D820H, D820N, D820V, D820Y, N822H, N822K, N822T, N822Y, Y823C, Y823D, Y823N, V825A, V825I, A829P, ***E839K***, L859P
LKB1:	A205T, D208N, C210*, Q214*, G215D, ***Q220****, ***E223****, F231L
MET:	D1246H, Y1248C, Y1248H, Y1253D, K1262R, ***M1268I***, ***M1268T***
PAK3:	T425S
PDGFRA:	R841S, D842*, D842I, D842V, D842Y, D846Y, Y849C, N870S
PDGFRB:	T882I
PKD3:	V716M
PRKCB1:	V496M
PSKH2:	K212I
RET:	E901K, R908K, G911D, ***M918T***, ***A919V***, ***E921K***, D925H
ROS:	F2138S
SGK2:	E259K
SIK:	G211S
TRKC:	R721F
TYRO3:	A709T

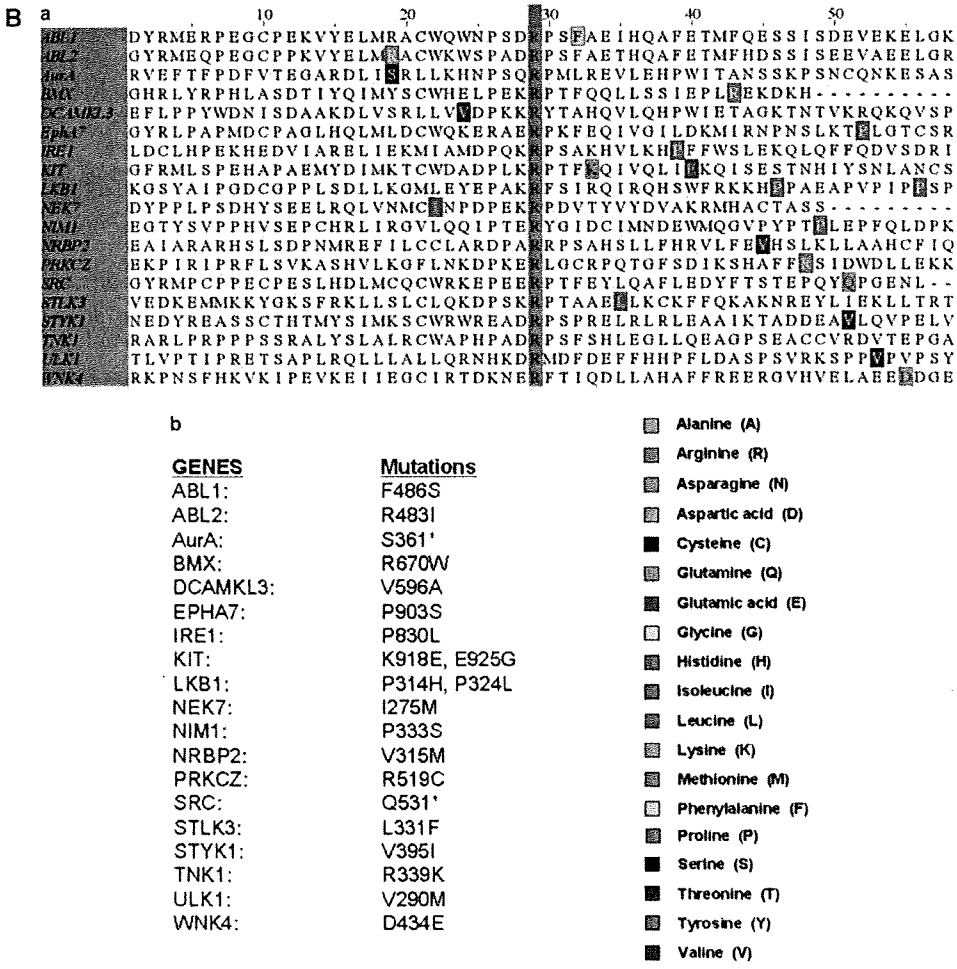

Figure 7 Continued.

important implications in the success of novel targeted inhibitors such as erlotinib (EGFR-TKI). Furthermore, knowledge of mutational correlation with inhibitor sensitivity-resistance would most likely facilitate more effective and 'personalized' targeted therapeutics development in cancer therapy. The clinical course of the patient where the somatic E884K mutation was identified (Choong *et al.*, 2006) suggested that different mutations of a target kinase, such as EGFR, may lead to differential responses to targeted kinase inhibitors. Alternatively, one may postulate that there might be differences in cerebrospinal fluid penetrance by TKIs that could potentially account for central nervous system failure with disease progression in the compartment on therapy (Jackman *et al.*, 2006). Our biochemical studies here now show that E884K mutation in-*cis* with L858R differentially altered inhibitor sensitivity when compared with L858R alone, through differential inhibition of the pro-survival AKT and STAT3 signaling pathways associated with altered induction of cleaved-PARP(Asp214). This is also shown to occur in an inhibitor-specific manner within the class of various

Figure 7 Survey of identified mutations at the conserved salt bridge ion pair in the human kinome (COSMIC). The COSMIC database for the human cancer genome resequencing was surveyed and screened for potential mutations identified at or near the conserved Glu(E)–Arg(R) salt bridge ion pair in the human kinome. (**A**) (a) Glu(E)884-EGFR and analogous alignment in the kinome. (b) List of the mutations identified in the kinome is included as reference. (**B**) (a) Arg(R)958-EGFR and analogous alignment in the kinome. (b) List of the mutations identified in the kinome is included as reference. The color code for the amino acids is included here. We have identified several kinases within the kinome that have mutations occurred at the Glu (E) residue, homologous to the E884-EGFR. These include KIT (E839K), RET (E921K) and LKB1 (E223*). These are all known oncogenic kinases that have dysregulated signaling in various human cancers, including GIST and hematological malignancies (KIT), papillary thyroid cancer (multiple endocrine neoplasm syndrome type 2) (RET) and lung adenocarcinoma (RET, LKB1). Whereas *KIT* and *RET* are oncogenes, *LKB1* has been shown to be a tumor-suppressor gene in lung cancer, and here we showed clustering of truncation mutations at and near the salt bridge ion pair as a result of a number of mostly nonsense mutations among some missense mutations. Although no mutation at E1271-*MET* was found, there are frequent clustered hotspots of mutations at its close vicinity: three amino-acid residues proximally at M1268 (M1268T/I). This is a known activating mutation of *MET* frequently associated with metastatic lesions promoting tumor motility and progression. The selected kinases with positive 'mutational hits' in our kinome bioinformatics screen are shown here for illustration.

ERBB family small-molecule inhibitors, including reversible single EGFR or dual inhibitors (gefitinib, erlotinib, lapatinib, 4557W, GW583340 and Tyrphostin-AG1478) and irreversible EGFR inhibitor (CL-387,785).

Moreover, the E884K alone and L858R + E884K double-mutant EGFR remained sensitive to EGF, and the E884K mutation cooperates with L858R when in-*cis* to enhance the mutational effects on downstream phosphoprotein activation. To date, essentially all mutational combinations involving L858R studied were found to exist in-*cis*, suggesting potential *cis* mutation-to-mutation cooperation in EGFR signaling and possibly tumorigenesis (Tam *et al.*, 2006). Interestingly, the double mutation L858R + E884K conferred a distinctly more sensitive response to EGF stimulation selectively in the MAPK-ERK1/2 cell proliferation pathway compared with either wild type, E884K alone or L858R alone. Hence, the double mutation L858R + E884K modulated downstream EGFR signaling differentially with distinctly different effects on the AKT (downregulated) and MAPK-ERK1/2 phosphorylation (upregulated). Moreover, E884K had a dominant effect over L858R, when in-*cis*, in these signaling modulatory effects. E884K, alone or in-*cis* with L858R, can also mediate induction of p-STAT3 (pY705) (important for STAT3 dimerization and transcriptional activation of target genes) and may have a role in differential regulation of STAT3 activation and thus nuclear translocation for transcriptional activity (Lo *et al.*, 2005). Our data also share some similarities to the recent findings that various activating 'gain-of-function' mutations of FLT3 showed differential downstream signaling activation along the STAT3, STAT5, AKT and MAPK-ERK1/2 pathways, whereas all induced FLT3 kinase activation constitutively (Frohling *et al.*, 2007). *EGFR* somatic doublet mutations are potentially more frequent than understood previously, with majority of them representing driver/driver mutations rather than driver/passenger mutations (Chen *et al.*, 2008). Future kinome-targeted therapies should take into account oncogenic effects of doublet mutations in the targets, and detailed analysis of the identified doublet mutations would be warranted.

Through sequence bioinformatics and structural analysis, we identified that the E884–R958 ion pair in EGFR kinase domain is highly conserved, by both sequence homology and structural salt-bridge formation, across the entire human kinome. Many of the protein kinases in the human kinome are 'druggable' therapeutic targets for various human cancers (Krause and Van Etten, 2005; Ma *et al.*, 2005a). This striking finding provides a structural basis for the potential mechanism of alteration of substrate specificity. This hypothesis is substantiated by our study using mutational disruption of the E884–R958 ion pair through an R958D substitution resulting in an opposite electrostatic charge between the wild-type and the mutant residue at codon 958. Similar differential sensitivity toward gefitinib (more sensitive) and erlotinib (more resistant) was observed in our *in vitro* EGFR inhibition study here. It is interesting to note that this salt bridge is located directly between two regions critical for normal EGFR activation, the intermolecular EGFR activation interface and the activation loop. Residue R958 falls between helices αH and αI and is proximal to the intermolecular EGFR activation interface recently revealed by structure-directed studies (Zhang *et al.*, 2006). Residue E884 is the conserved glutamate of the MALE motif (MAPE in PKA) and falls within helix αEF at the C terminus of the activation loop. This salt bridge helps to orientate helix αEF. In the recent EGFR kinase domain crystal structure bound to a peptide substrate analog (PDB accession code: 2GS6) (Zhang *et al.*, 2006), helix αEF packs against the substrate analog, suggesting that disruption of the salt bridge by an acquired E884K mutation could influence substrate recognition and binding. The acquisition of a lysine at codon 884 may therefore bring about local conformation disruptions that alter EGFR interactions with downstream substrates. Although we did not identify further E884K mutation (or any mutations involving R958 residue) in *EGFR* from the Japanese patients tumor sample cohort, the results of our study may have implication on the potential impact of cancer-associated mutations that may interrupt the integrity of the salt bridge of a kinase. As the human kinome is a rich source of 'druggable' targets, we extended our search through bioinformatics data-mining from the COSMIC human cancer genome resequencing project. To this end, we identified several proximal ion pair residue substitutions recorded in the COSMIC database at the E884 (EGFR) homologous residue, in the oncogenic kinases KIT and RET as well as in the tumor-suppressor LKB1 (also known as STK11). Mutations at the neighboring residues of the conserved motif MAPE(884), as exemplified in FAK-A612V, MET-M1268I/T, RET-M918T and RET-A919V, as well as the truncational nonsense mutation in LKB1-Q220*, were also identified from the COSMIC database. Furthermore, the juxtaposing proximal region to the MAPE(884) conserved motif in the kinome also appears to harbor mutational hotspots in the human cancer genome. Nonetheless, the significance of these mutations with respect to the kinase structure and signaling function is not clear. Although KIT has been extensively characterized with an established oncogenic role in some hematological malignancies and GIST, it has not been found to play a key role in lung cancer. However, recent studies have implicated interesting oncogenic role of RET (Thomas *et al.*, 2007), FAK (Ma *et al.*, 2007; Rikova *et al.*, 2007), MET (Ma *et al.*, 2005a) and tumor-suppressor role of LKB1 (Ji *et al.*, 2007) in lung cancer.

Recently, better understanding of signaling network interactions between EGFR and MET is beginning to emerge (Guo *et al.*, 2008; Tang *et al.*, 2008). MET genomic oncogenic amplification has also been identified to correlate with acquired resistance to EGFR inhibitors (gefitinib/erlotinib) with or without T790M-*EGFR* mutation (Bean *et al.*, 2007; Engelman *et al.*, 2007). Numerous kinase domain mutations of *MET* have been identified in previous studies, many of them shown to be activating and most frequently found in

metastatic tumor lesions compared with the primaries (Di Renzo *et al.*, 2000). The E1271–MET conserved ion pair residue occurs within the conserved MALE motif, where M1268 is a mutational hotspot frequently found substituted in human cancers (M1268T/I). This is a known activating mutation of *MET* frequently associated with metastatic lesions promoting tumor motility and progression. Our results here demonstrate that E1271K-MET effectuated differential effect on sensitivity toward the two preclinical MET inhibitors, SU11274 (unchanged) and PHA665752 (sensitizing). Hence, mutations in the kinase domain of MET may play a role in modulating the inhibitory spectrum of MET inhibitors, similar to what is established in EGFR-targeted therapy using gefitinib/erlotinib. Whether these mutationally specific differences in inhibitor sensitivity would eventually be clinically relevant is not clear at present and should be a focus of future research. MET is emerging as an important therapeutic target in cancer therapy beyond EGFR. More detailed studies to better define the relative role of kinase mutations in *MET* and how they can modulate inhibitor sensitivity would be warranted. Furthermore, nonkinase mutations of *MET*, in the extracellular sema domain and the short cytoplasmic juxtamembrane domain, have been identified to be important in lung cancer and mesothelioma (Ma *et al.*, 2003a, 2005a; Jagadeeswaran *et al.*, 2006). Little is known about the correlation of inhibitor sensitivity with these nonkinase mutations, and they should be included in future studies. Bellon *et al.* (2008) recently compared the crystal structures of a novel MET inhibitor AM7, and that of SU11274 when bound to the unphosphorylated form of MET kinase. They identified a novel binding mode of a MET inhibitor AM7 compared with SU11274 and raised the possibility of designing TKIs that have improved specific activity and specificity toward different mutant profiles in different cancers; hence 'mutationally-targeted inhibitors'.

Although the role of kinase domain mutations in modulating the sensitivity-resistance to small-molecule inhibitors, in the case of BCR/ABL, KIT and EGFR, has been quite extensively studied, in-depth understanding of the relative role of mutations in other target kinases, such as MET, RET and FAK in determining specific inhibitor sensitivity is still largely lacking. The ion pair formed by residues E884 and R958 in the EGFR kinase domain is a highly conserved feature in the human kinome, and mutations of this conserved ion pair may result in conformational changes that alter kinase substrate recognition. The discovery that disruption of the conserved E884–R958 ion pair affects EGFR signal transduction and inhibitor sensitivity indicates the clinical importance of *in vitro* and biochemical analysis for all documented resistance mutations. Our analysis also suggests that targeted therapy using small-molecule inhibitors should take into account potential cooperative effects of multiple intramolecular kinase mutations. As the number of targeted TKIs available increases, it is anticipated that a 'personalized' approach to cancer therapy on the basis of knowledge of the activating mutations present should improve the efficacy of these treatments.

Materials and methods

Plasmid constructs and site-directed mutagenesis
The plasmids pcDNA3.1 containing the full-length wild-type *EGFR* and the L858R-*EGFR* cDNA insert was a generous gift from Dr Stanley Lipkowitz (NIH/NCI). The generation of the kinase domain missense mutations of *EGFR*, E884K, L858R + E884K and L858R + R958D were performed using the QuikChange Site-Directed Mutagenesis XL II kit (Stratagene, La Jolla, CA, USA) as described previously (Choong *et al.*, 2006). The E1271K mutation of *MET* was introduced into the wild-type *MET* plasmid (Ma *et al.*, 2003a). Incorporation of the correct mutations was confirmed by direct DNA sequencing of the constructs.

Cell culture and transfection
COS-7 cells were grown as described previously (Choong *et al.*, 2006). Transfection method was described in Supplementary Materials and methods.

Cell proliferation and cytotoxicity assays
Cell proliferation and cytotoxicity assays were performed using tetrazolium compound-based CellTiter 96 AQ_{ueous} One Solution Cell Proliferation (MTS) assay (Promega) (see Supplementary Materials and methods).

Preparation of cell lysates and immunoblotting
Whole-cell lysates were extracted, separated by 7.5% SDS–polyacrylamide gel electrophoresis , immunoblotted using the various primary antibodies indicated and developed with SuperSignal West Pico Chemiluminescent Substrate (Pierce, Rockford, IL, USA) as described previously (Choong *et al.*, 2006). The following primary antibodies were used: phosphotyrosine (4G10, Upstate Biotechnology, Lake Placid, NY, USA), phospho-EGFR (Y1068) (BioSource International, Camarillo, CA, USA), EGFR (Santa Cruz Biotechnology, Santa Cruz, CA, USA), phospho-STAT3 (Y705) (Cell Signaling, Danvers, MA, USA), STAT3 (Zymed, South San Francisco, CA, USA), phospho-AKT (S473) (Cell Signaling), AKT (Biosource International), phospho-ERK1/2 (T202/Y204) (Cell Signaling), ERK1/2 (Biosource International), cleaved-PARP(Asp214) (cleaved-poly (ADP-ribose) polymerase (Asp214)) (Cell Signaling) and β-actin (Santa Cruz Biotechnology).

Chemicals
The details regarding the EGFR TKIs and MET TKIs used in this study are described in the Supplementary Materials and methods.

Lung tumor genomic DNA extraction and DNA sequencing
Genomics DNA was extracted using standard techniques from 67 non-small-cell lung cancer patients treated from July 1995 to March 2003 at Osaka Prefectural Medical Center for Respiratory and Allergic Disease (Osaka, Japan). All tumor samples were used in accordance with Institutional Review Board protocol, with patients' informed consent wherever necessary. Screening for mutations within exon 22 (harboring E884) and exon 23 (harboring R958) was performed using standard single-strand conformational polymorphism analysis, followed by direct DNA sequencing when indicated (for details, see Supplementary Materials and methods).

Bioinformatics sequence analysis

Multiple sequence alignments of kinase domains in the human kinome were performed for 321 human kinase domains. The positions of the conserved glutamate (E) and arginine (R) residues are colored purple and those of EGFR are indicated in red. FASTA files for human kinase domains were obtained from the kinase database at Sugen/Salk (Kinbase, La Jolla, CA, USA) and aligned with the AliBee multiple sequence alignment program (GeneBee) (Brodsky *et al.*, 1992) using Clustal format. Resulting alignments were colored using JalView 2.2 (Clamp *et al.*, 2004) according to sequence conservation (BLOSUM62). In addition, the amino-acid sequences from a selected list of 32 diverse human protein kinases were obtained from the ENSEMBL database (www.ensembl.org). The amino-acid sequences of these kinase domains were analysed and aligned using the EMBL-EBI online CLUSTALW software (www.ebi.ac.uk/clustalw).

Structural analysis

EGFR crystal structures (PDB accession codes 1M17, 1XKK and 2GS6) (Stamos *et al.*, 2002; Wood *et al.*, 2004; Zhang *et al.*, 2006) were analysed using the program O (Jones *et al.*, 1991). Superposition of the EGFR kinase domain with the catalytic domains of diverse kinases was performed to study the structural conservation of a buried Glu(E)–Arg(R) ion pair. The crystal structure of EGFR tyrosine kinase (PDB accession code: 1M17) (Stamos *et al.*, 2002) was superimposed with the catalytic kinase domains of human CDK2 (PDB accession code: 1VYW) (Pevarello *et al.*, 2004), human JNK3 (PDB accession code: 1PMQ) (Scapin *et al.*, 2003), human insulin receptor kinase (PDB accession code: 1IR3) (Hubbard, 1997), ZAP-70 tyrosine kinase (PDB accession code: 1U59) (Jin *et al.*, 2004), LCK kinase (PDB accession code: 1QPD) (Zhu *et al.*, 1999) and MET (PDB accession code: 2RFS) (Bellon *et al.*, 2008) using Cα atoms in the program DeepView/Swiss-PdbViewer v3.7. Figures were prepared using the program PYMOL (www.pymol.org).

Abbreviations

COSMIC, catalogue of somatic mutations in cancer; EGFR, epidermal growth factor receptor; MAPK (ERK1/2), mitogen-activated protein kinase (extracellular signaling-regulated kinase 1/2); STAT3, signal transducer and activator of transcription 3; TKI, tyrosine kinase inhibitor.

Acknowledgements

Patrick C Ma is supported by NIH/National Cancer Institute-K08 Career Development Award (5K08CA102545-04), American Cancer Society (Ohio)-Institutional Research Grant (IRG-91-022, Case Comprehensive Cancer Center) and Ohio Cancer Research Associates (Give New Ideas A Chance) Grant Award. Titus J Boggon is an American Society of Hematology Junior Faculty Scholar. Edward T Petri is supported by an NIH/National Cancer Institute T32 training Grant (5T32CA009085-32). We thank Dr Zhenghe J Wang (Department of Genetics, Case Western Reserve University) for critically reading the manuscript and for helpful suggestions.

References

Bean J, Brennan C, Shih JY, Riely G, Viale A, Wang L *et al.* (2007). MET amplification occurs with or without T790M mutations in EGFR mutant lung tumors with acquired resistance to gefitinib or erlotinib. *Proc Natl Acad Sci USA* **104**: 20932–20937.

Bellon SF, Kaplan-Lefko P, Yang Y, Zhang Y, Moriguchi J, Rex K *et al.* (2008). c-Met inhibitors with novel binding mode show activity against several hereditary papillary renal cell carcinoma related mutations. *J Biol Chem* **283**: 2675–2683.

Brodsky LI, Vasiliev AV, Kalaidzidis YL, Osipov YS, Tatuzov RL, Feranchuk SI. (1992). GeneBee: the program package for biopolymer structure analysis. *Dimacs* **8**: 127–139.

Chen Z, Feng J, Saldivar JS, Gu D, Bockholt A, Sommer SS (2008). EGFR somatic doublets in lung cancer are frequent and generally arise from a pair of driver mutations uncommonly seen as singlet mutations: one-third of doublets occur at five pairs of amino acids. *Oncogene* **27**: 4336–4343.

Choong NW, Dietrich S, Seiwert TY, Tretiakova MS, Nallasura V, Davies GC *et al.* (2006). Gefitinib response of erlotinib-refractory lung cancer involving meninges—role of EGFR mutation. *Nat Clin Pract Oncol* **3**: 50–57; quiz 51 p following 57.

Clamp M, Cuff J, Searle SM, Barton GJ. (2004). The Jalview Java alignment editor. *Bioinformatics* **20**: 426–427.

Di Renzo MF, Olivero M, Martone T, Maffe A, Maggiora P, Stefani AD *et al.* (2000). Somatic mutations of the MET oncogene are selected during metastatic spread of human HNSC carcinomas. *Oncogene* **19**: 1547–1555.

Engelman JA, Zejnullahu K, Mitsudomi T, Song Y, Hyland C, Park JO *et al.* (2007). MET amplification leads to gefitinib resistance in lung cancer by activating ERBB3 signaling. *Science* **316**: 1039–1043.

Frohling S, Scholl C, Levine RL, Loriaux M, Boggon TJ, Bernard OA *et al.* (2007). Identification of driver and passenger mutations of FLT3 by high-throughput DNA sequence analysis and functional assessment of candidate alleles. *Cancer Cell* **12**: 501–513.

Guo A, Villen J, Kornhauser J, Lee KA, Stokes MP, Rikova K *et al.* (2008). Signaling networks assembled by oncogenic EGFR and c-Met. *Proc Natl Acad Sci USA* **105**: 692–697.

Hubbard SR. (1997). Crystal structure of the activated insulin receptor tyrosine kinase in complex with peptide substrate and ATP analog. *Embo J* **16**: 5572–5581.

Jackman DM, Holmes AJ, Lindeman N, Wen PY, Kesari S, Borras AM *et al.* (2006). Response and resistance in a non-small-cell lung cancer patient with an epidermal growth factor receptor mutation and leptomeningeal metastases treated with high-dose gefitinib. *J Clin Oncol* **24**: 4517–4520.

Jagadeeswaran R, Ma PC, Seiwert TY, Jagadeeswaran S, Zumba O, Nallasura V *et al.* (2006). Functional analysis of c-Met/hepatocyte growth factor pathway in malignant pleural mesothelioma. *Cancer Res* **66**: 352–361.

Ji H, Ramsey MR, Hayes DN, Fan C, McNamara K, Kozlowski P *et al.* (2007). LKB1 modulates lung cancer differentiation and metastasis. *Nature* **448**: 807–810.

Jin L, Pluskey S, Petrella EC, Cantin SM, Gorga JC, Rynkiewicz MJ *et al.* (2004). The three-dimensional structure of the ZAP-70 kinase domain in complex with staurosporine: implications for the design of selective inhibitors. *J Biol Chem* **279**: 42818–42825.

Jones TA, Zou JY, Cowan SW, Kjeldgaard M. (1991). Improved methods for building protein models in electron density maps and the location of errors in these models. *Acta Crystallogr A* **47**(Part 2): 110–119.

Kobayashi S, Boggon TJ, Dayaram T, Janne PA, Kocher O, Meyerson M *et al.* (2005). EGFR mutation and resistance of non-small-cell lung cancer to gefitinib. *N Engl J Med* **352**: 786–792.

Krause DS, Van Etten RA. (2005). Tyrosine kinases as targets for cancer therapy. *N Engl J Med* **353**: 172–187.

Lo HW, Hsu SC, Ali-Seyed M, Gunduz M, Xia W, Wei Y *et al.* (2005). Nuclear interaction of EGFR and STAT3 in the activation of the iNOS/NO pathway. *Cancer Cell* **7**: 575–589.

Lynch TJ, Bell DW, Sordella R, Gurubhagavatula S, Okimoto RA, Brannigan BW *et al.* (2004). Activating mutations in the epidermal growth factor receptor underlying responsiveness of non-small-cell lung cancer to gefitinib. *N Engl J Med* **350**: 2129–2139.

Ma PC, Jagadeeswaran R, Jagadeesh S, Tretiakova MS, Nallasura V, Fox EA *et al.* (2005a). Functional expression and mutations of c-Met and its therapeutic inhibition with SU11274 and small interfering RNA in non-small cell lung cancer. *Cancer Res* **65**: 1479–1488.

Ma PC, Kijima T, Maulik G, Fox EA, Sattler M, Griffin JD *et al.* (2003a). c-MET mutational analysis in small cell lung cancer: novel juxtamembrane domain mutations regulating cytoskeletal functions. *Cancer Res* **63**: 6272–6281.

Ma PC, Maulik G, Christensen J, Salgia R. (2003b). c-Met: structure, functions and potential for therapeutic inhibition. *Cancer Metastasis Rev* **22**: 309–325.

Ma PC, Schaefer E, Christensen JG, Salgia R. (2005b). A selective small molecule c-MET Inhibitor, PHA665752, cooperates with rapamycin. *Clin Cancer Res* **11**: 2312–2319.

Ma PC, Tretiakova MS, Nallasura V, Jagadeeswaran R, Husain AN, Salgia R. (2007). Downstream signalling and specific inhibition of c-MET/HGF pathway in small cell lung cancer: implications for tumour invasion. *Br J Cancer* **97**: 368–377.

Mazzone M, Comoglio PM. (2006). The Met pathway: master switch and drug target in cancer progression. *FASEB J* **20**: 1611–1621.

Paez JG, Janne PA, Lee JC, Tracy S, Greulich H, Gabriel S *et al.* (2004). EGFR mutations in lung cancer: correlation with clinical response to gefitinib therapy. *Science* **304**: 1497–1500.

Peruzzi B, Bottaro DP. (2006). Targeting the c-Met signaling pathway in cancer. *Clin Cancer Res* **12**: 3657–3660.

Pevarello P, Brasca MG, Amici R, Orsini P, Traquandi G, Corti L *et al.* (2004). 3-Aminopyrazole inhibitors of CDK2/cyclin A as antitumor agents. 1. Lead finding. *J Med Chem* **47**: 3367–3380.

Rikova K, Guo A, Zeng Q, Possemato A, Yu J, Haack H *et al.* (2007). Global survey of phosphotyrosine signaling identifies oncogenic kinases in lung cancer. *Cell* **131**: 1190–1203.

Scapin G, Patel SB, Lisnock J, Becker JW, LoGrasso PV. (2003). The structure of JNK3 in complex with small molecule inhibitors: structural basis for potency and selectivity. *Chem Biol* **10**: 705–712.

Shigematsu H, Gazdar AF. (2006). Somatic mutations of epidermal growth factor receptor signaling pathway in lung cancers. *Int J Cancer* **118**: 257–262.

Shinomiya N, Gao CF, Xie Q, Gustafson M, Waters DJ, Zhang YW *et al.* (2004). RNA interference reveals that ligand-independent met activity is required for tumor cell signaling and survival. *Cancer Res* **64**: 7962–7970.

Smolen GA, Sordella R, Muir B, Mohapatra G, Barmettler A, Archibald H *et al.* (2006). Amplification of MET may identify a subset of cancers with extreme sensitivity to the selective tyrosine kinase inhibitor PHA-665752. *Proc Natl Acad Sci USA* **103**: 2316–2321.

Stamos J, Sliwkowski MX, Eigenbrot C. (2002). Structure of the epidermal growth factor receptor kinase domain alone and in complex with a 4-anilinoquinazoline inhibitor. *J Biol Chem* **277**: 46265–46272.

Tam IY, Chung LP, Suen WS, Wang E, Wong MC, Ho KK *et al.* (2006). Distinct epidermal growth factor receptor and KRAS mutation patterns in non-small cell lung cancer patients with different tobacco exposure and clinicopathologic features. *Clin Cancer Res* **12**: 1647–1653.

Tang Z, Du R, Jiang S, Wu C, Barkauskas DS, Richey J *et al.* (2008). Dual MET-EGFR combinatorial inhibition against T790M-EGFR-mediated erlotinib-resistant lung cancer. *Br J Cancer* **99**: 911–922, 2008.

Thomas RK, Baker AC, Debiasi RM, Winckler W, Laframboise T, Lin WM *et al.* (2007). High-throughput oncogene mutation profiling in human cancer. *Nat Genet* **39**: 347–351.

Wood ER, Truesdale AT, McDonald OB, Yuan D, Hassell A, Dickerson SH *et al.* (2004). A unique structure for epidermal growth factor receptor bound to GW572016 (Lapatinib): relationships among protein conformation, inhibitor off-rate, and receptor activity in tumor cells. *Cancer Res* **64**: 6652–6659.

Zhang X, Gureasko J, Shen K, Cole PA, Kuriyan J. (2006). An allosteric mechanism for activation of the kinase domain of epidermal growth factor receptor. *Cell* **125**: 1137–1149.

Zhu X, Kim JL, Newcomb JR, Rose PE, Stover DR, Toledo LM *et al.* (1999). Structural analysis of the lymphocyte-specific kinase Lck in complex with non-selective and Src family selective kinase inhibitors. *Structure* **7**: 651–661.

Supplementary Information accompanies the paper on the Oncogene website (http://www.nature.com/onc)

Inhibition of Insulin-Like Growth Factor 1 Receptor by CP-751,871 Radiosensitizes Non–Small Cell Lung Cancer Cells

Tsutomu Iwasa,[1] Isamu Okamoto,[1] Minoru Suzuki,[2] Erina Hatashita,[1] Yuki Yamada,[1] Masahiro Fukuoka,[3] Koji Ono,[2] and Kazuhiko Nakagawa[1]

Abstract **Purpose:** Therapeutic strategies that target the insulin-like growth factor I receptor (IGF-1R) hold promise for a wide variety of cancers. We have now investigated the effect of CP-751,871, a fully human monoclonal antibody specific for IGF-IR, on the sensitivity of human non–small cell lung cancer (NSCLC) cell lines to radiation.

Experimental Design: The radiosensitizing effect of CP-751,871 was evaluated on the basis of cell death, clonogenic survival, and progression of tumor xenografts. Radiation-induced damage was evaluated by immunofluorescence analysis of the histone γ-H2AX and Rad51.

Results: A clonogenic survival assay revealed that CP-751,871 increased the sensitivity of NSCLC cells to radiation *in vitro*. CP-751,871 inhibited radiation-induced IGF-IR signaling, and potentiated the radiation-induced increases both in the number of apoptotic cells and in the activity of caspase-3. Immunofluorescence analysis of the histone γ-H2AX and Rad51 also showed that CP-751,871 inhibited the repair of radiation-induced DNA double-strand breaks. Finally, combination therapy with CP-751,871 and radiation delayed the growth of NSCLC tumor xenografts in nude mice to a greater extent than did either treatment modality alone.

Conclusions: These results show that CP-751,871 sensitizes NSCLC cells to radiation both *in vitro* and *in vivo*, and that this effect of CP-751,871 is likely attributable to the inhibition of DNA repair and enhancement of apoptosis that result from attenuation of IGF-IR signaling. Combined treatment with CP-751,871 and radiation thus warrants further investigation in clinical trials as a potential anticancer strategy. (Clin Cancer Res 2009;15(16):5117–25)

The insulin-like growth factor I receptor (IGF-IR) is a receptor tyrosine kinase that contributes to the regulation of cell growth, transformation, and apoptosis, and plays an important role in tumor cell proliferation and survival (1, 2). Antisense oligonucleotides, inhibitory peptides, and kinase inhibitors that target IGF-IR, as well as dominant negative mutant and soluble forms of the receptor have been found to inhibit the proliferation of tumor cell lines *in vitro* and in experimental mouse models (3–7). Targeting of IGF-IR is thus a promising strategy for cancer therapy. The two most investigated therapeutic approaches in preclinical models are based on specific tyrosine kinase inhibitors and monoclonal antibodies (mAb; ref. 7–11). Although IGF-IR tyrosine kinase inhibitors have a high affinity for IGF-IR, cross-inhibition of the insulin receptor remains a problem because of the high level of sequence similarity between the tyrosine kinase domains of these two receptors (12). Such cross-inhibition has the potential to induce symptoms of diabetes in treated individuals (13). In contrast, antibodies that target the extracellular domain of IGF-IR are highly selective for IGF-IR. Currently available antibodies to IGF-IR are of the IgG1 and IgG2 isotypes (7–10). These two isotypes differ in that IgG2 antibodies manifest a longer half-life in humans, whereas IgG1 antibodies are more effective at eliciting immune cell effector functions (antibody-dependent cytotoxicity). CP-751,871 is a potent, fully human IgG2 mAb specific for IGF-IR that inhibits tumor growth as a single agent and enhances the efficacy of other anticancer agents in human tumor xenograft models (10). CP-751,871 is thus an attractive candidate drug for cancer therapy, and clinical trials of this agent in combination with chemotherapy are currently underway for certain types of cancer.

Overexpression of IGF-IR in NIH 3T3 fibroblasts confers radioresistance in preclinical models (14). Expression and activation of IGF-IR have also been associated with resistance to

[1]Department of Medical Oncology, Kinki University School of Medicine, Osaka-Sayama, Osaka, Japan; [2]Radiation Oncology Research Laboratory, Research Reactor Institute, Kyoto University, Sennan-gun, Osaka, Japan; and [3]Department of Medical Oncology, Kinki University School of Medicine, Sakai Hospital, Sakai, Osaka, Japan

Received 2/24/09; revised 4/30/09; accepted 5/18/09; published OnlineFirst 8/11/09.

The costs of publication of this article were defrayed in part by the payment of page charges. This article must therefore be hereby marked *advertisement* in accordance with 18 U.S.C. Section 1734 solely to indicate this fact.

Note: Supplementary data for this article are available at Clinical Cancer Research Online (http://clincancerres.aacrjournals.org/).

Requests for reprints: Isamu Okamoto, Department of Medical Oncology, Kinki University School of Medicine, 377-2 Ohno-higashi, Osaka-Sayama, Osaka 589-8511, Japan. Phone: 81-72-366-0221; Fax: 81-72-360-5000; E-mail: chi-okamoto@dotd.med.kindai.ac.jp.

doi:10.1158/1078-0432.CCR-09-0478

Translational Relevance

Targeting of IGF-IR is a promising strategy for cancer therapy. CP-751,871 is a fully human monoclonal antibody specific for IGF-IR that inhibits tumor growth in human tumor xenograft models *in vivo*. Although phase II studies of CP-751,871 in combination with chemotherapy are currently underway for certain types of cancer, the effects of CP-751,871 in combination with radiation have not been described. We now show a radiosensitizing effect of CP-751,871 in non–small cell lung cancer cell lines *in vitro* and *in vivo*. Our preclinical data provide a rationale for future clinical investigation of the therapeutic efficacy of CP-751,871 in combination with radiotherapy.

radiotherapy in cancer patients (15). Inhibition of IGF-IR by antisense oligonucleotides, IGF-IR tyrosine kinase inhibitors, or mouse mAbs to the receptor has been shown to enhance the radiosensitivity of tumor cells (16–18). However, the effects of fully human mAbs to IGF-IR on radiosensitivity in cancer cells have not been characterized in detail. We have now examined the effects of the combination of CP-751,871 and radiation on non–small cell lung cancer (NSCLC) cell lines as well as the mechanism responsible for enhancement of radiosensitivity by CP-751,871.

Materials and Methods

Cell culture and reagents. The human NSCLC cell lines National Cancer Institute (NCI)-H292 (H292), NCI-H460 (H460), NCI-H1299 (H1299), LK-2, and NCI-H1975 (H1975) were obtained from American Type Culture Collection (Manassas, VA). The cells were cultured under an atmosphere of 5% CO_2 at 37°C in RPMI 1640 (Sigma, St. Louis, MO) supplemented with 10% fetal bovine serum. Recombinant human IGF-I was obtained from R&D Systems (Minneapolis, MN). CP-751,871 was kindly provided by Pfizer Global Research & Development (Groton, CT).

Immunoblot analysis. Cells were washed twice with ice-cold PBS, and then lysed in a solution containing 20 mmol/L Tris-HCl (pH 7.5), 150 mmol/L NaCl, 1 mmol/L EDTA, 1% Triton X-100, 2.5 mmol/L sodium pyrophosphate, 1 mmol/L phenylmethylsulfonyl fluoride, and leupeptin (1 μg/mL). The protein concentration of lysates was determined with the Bradford reagent (Bio-Rad, Hercules, CA), and equal amounts of protein were subjected to SDS-PAGE on a 7.5% gel. The separated proteins were transferred to a nitrocellulose membrane, which was then exposed to 5% nonfat dried milk in PBS for 1 h at room temperature before incubation overnight at 4°C with rabbit polyclonal antibodies to phosphorylated human IGF-IR (1:1,000 dilution; Cell Signaling, Beverly, MA), to human IGF-IR (1:1,000 dilution; MBL International, Woburn, MA), to phosphorylated human AKT (1:1,000 dilution; Cell Signaling), to human AKT (1:1,000 dilution; Cell Signaling), or to β-actin (1:500 dilution; Sigma). The membrane was then washed with PBS containing 0.05% Tween 20 before incubation for 1 h at room temperature with horseradish peroxidase–conjugated goat antibodies to rabbit IgG (Sigma). Immune complexes were finally detected with chemiluminescence reagents (Perkin-Elmer Life Sciences, Boston, MA).

Flow cytometric analysis of surface IGF-IR expression. Cells (2×10^6) were stained for 2 h at 4°C with an R-phycoerythrin–conjugated mAb to IGF-IR (BD Biosciences, San Jose, CA) or with an isotype-matched control antibody (BD Biosciences). The cells were washed thrice before measurement of fluorescence with a flow cytometer (FACScalibur; Becton Dickinson, San Jose, CA).

Clonogenic survival assay. Exponentially growing cells in 25-cm^2 flasks were harvested by exposure to trypsin and counted. They were diluted serially to appropriate densities, and plated in triplicate in 25-cm^2 flasks containing 10 mL of complete medium in the presence of 50 nmol/L CP-751,871 or vehicle (PBS) before exposure at room temperature to various doses of radiation with a ^{60}Co irradiator at a rate of ~0.82 Gy/min. After incubation for 4 h, the cells were washed with PBS, cultured in antibody-free medium for 10 to 14 d, fixed with methanol/acetic acid (10:1, volume per volume), and stained with crystal violet. Colonies containing >50 cells were counted. The surviving fraction was calculated as: (mean number of colonies)/(number of inoculated cells × plating efficiency). Plating efficiency was defined as the mean number of colonies divided by the number of inoculated cells for the corresponding nonirradiated cells. The surviving fraction for combined treatment was corrected by that for CP-751,871 treatment alone. The dose enhancement factor was then calculated as the dose (Gy) of radiation that yielded a surviving fraction of 0.1 for vehicle-treated cells divided by that for CP-751,871–treated cells (after correction for drug toxicity).

Detection of apoptotic cells. Cells were fixed with 4% paraformaldehyde for 1 h at room temperature, after which a minimum of 1,000 cells per sample was evaluated for apoptosis with the use of the terminal deoxyribonucleotide transferase–mediated nick-end labeling technique (*In situ* Cell Death Detection kit; Boehringer Mannheim, Mannheim, Germany).

Assay of caspase-3 activity. The activity of caspase-3 in cell lysates was measured with a CCP32/Caspase-3 Fluometric Protease Assay kit (MBL). Fluorescence attributable to cleavage of the Asp-Glu-Val-Asp-7-amino-4-trifluoromethyl coumarin (DEVD-AFC) substrate was measured at excitation and emission wavelengths of 390 and 460 nm, respectively.

Immunofluorescence staining of γ-H2AX and Rad51. Cells were grown to 50% confluence in 2-well Lab-Tec Chamber Slides (Nunc, Naperville, IL), deprived of serum overnight, exposed to 10 Gy of radiation in the presence of 50 nmol/L CP-751,871 or vehicle in serum-free medium, incubated for 4 h, and then cultured for various times in complete medium alone. The cells were fixed with 4% paraformaldehyde for 10 min at room temperature, permeabilized with 0.1% Triton X-100 for 10 min at 4°C, and exposed to 5% nonfat dried milk for 10 min at room temperature. They were then washed with PBS and stained overnight at 4°C with mouse mAbs to γ-H2AX (Upstate Biotechnology, Lake Placid, NY) at a dilution of 1:300 and with rabbit polyclonal antibodies to Rad51 (Oncogene Research Products, San Diego, CA) at a dilution of 1:500. Immune complexes were detected by incubation of the slides for 1 h at room temperature with Alexa 488–labeled goat antibodies to mouse IgG (Molecular Probes, Eugene, OR) at a dilution of 1:700 and with Texas red–labeled goat antibodies to rabbit IgG (Vector Laboratories, Burlingame, CA) at a dilution of 1:300. The slides were mounted in fluorescence mounting medium (Dako Cytomation, Hamburg, Germany), and fluorescence signals were visualized with a confocal laser scanning microscope (Axiovert 200M; Carl Zeiss, Oberkochen, Germany) equipped with the LSM 5 PASCAL system (Carl Zeiss). Three random fields, each containing at least 50 cells, were examined at a magnification of ×100, and the percentage of cells containing >5 Rad51 foci per nucleus was determined (19). Nuclei containing ≥10 immunoreactive foci were counted as positive for γ-H2AX, and the percentage of positive cells was calculated (20).

Evaluation of tumor growth in vivo. All animal studies were done in accordance with the Recommendations for Handling of Laboratory Animals for Biomedical Research compiled by the Committee on Safety and Ethical Handling Regulations for Laboratory Animal Experiments, Kyoto University. The ethical procedures followed met the requirements of the United Kingdom Co-ordinating Committee on Cancer Research guidelines (21). Tumor cells (2×10^6) were implanted into the right hind leg of 6-week-old female athymic nude mice (BALB/c *nu/nu*).

Tumor volume was determined from caliper measurement of tumor length (L) and width (W) according to the formula $LW^2/2$. Treatment was initiated when tumors in each group of animals achieved an average volume of ~200 to 250 mm^3. Treatment groups (each containing five mice) consisted of vehicle control (PBS), CP-751,871 alone, vehicle plus radiation, and CP-751,871 plus radiation. CP-751,871 was given i.p. in a single dose of 500 μg per mouse; mice in the control and radiation-alone groups were treated with vehicle (PBS). Mice in the radiation groups received 10 Gy of radiation from a ^{60}Co irradiator either as a single fraction on day 1 of drug treatment or fractionated over 5 consecutive days (days 1 to 5); the radiation was targeted at the tumor, with the remainder of the body shielded with lead. Growth delay (GD) was calculated as the time required to achieve a 5-fold increase in volume for treated tumors minus that for control tumors. The enhancement factor was then determined as:

$$(GD_{combination} - GD_{CP-751,871})/GD_{radiation}.$$

Statistical analysis. Data are presented as means ± SD and were compared between groups with the unpaired Student's *t* test. A *P*-value of <0.05 was considered statistically significant. The effect of the combination of CP-751,871 and radiation on cell survival was assessed by calculation of the combination index with the use of CalcSyn software Biosoft (Cambridge, United Kingdom). Derived from the median-effect principle of Chou and Talalay (22), the combination index provides a quantitative measure of the degree of interaction between ≥2 agents. A combination index of 1 denotes an additive interaction, of >1 denotes antagonism, and of <1 denotes synergy.

Results

IGF-IR expression in NSCLC cells. Immunoblot analysis revealed that IGF-IR was expressed in all human NSCLC cell lines tested (Fig. 1A). Flow cytometry further showed that IGF-IR was expressed at the cell surface in each of these cell lines (Fig. 1B).

CP-751,871 inhibits IGF-IR signaling by blocking IGF-I binding and inducing receptor down-regulation. The efficacy of treatment with mAbs to IGF-IR is thought to be attributable in part to the prevention of ligand binding to the receptor (9). We examined the effects of CP-751,871 on IGF-IR phosphorylation and on activation of the downstream effector AKT induced by ligand stimulation. Immunoblot analysis showed that IGF-I induced marked phosphorylation both of IGF-IR and of the protein kinase AKT in H460 cells, whereas CP-751,871 largely prevented these effects of IGF-I (Fig. 1C). Antibodies to IGF-IR have also been shown to induce receptor down-regulation (12). We also found that CP-751,871 induced a time-dependent decrease in the abundance of IGF-IR in H460 cells, with this effect being pronounced after only 2 hours (Fig. 1D). These results thus suggested that CP-751,871 suppresses IGF-IR signaling through both the direct antagonism of ligand binding and the induction of receptor down-regulation.

***CP-751,871 sensitizes NSCLC cells to radiation* in vitro.** To determine whether CP-751,871 affects the sensitivity of NSCLC cells to radiation, we did a clonogenic survival assay. CP-751,871 enhanced the cytotoxic effect of radiation in all tested cell lines (Fig. 2A), with dose enhancement factors of 1.28, 1.20, 1.27, 1.20, and 1.25 for H460, H1299, H292, LK-2, and H1975 cells, respectively. We examined whether the interaction between CP-751,871 and radiation was additive or synergistic by calculating the combination index based on the median-effect principle of Chou and Talalay (22). Synergism with CP-751,871 was apparent at radiation doses of 4, 6, and

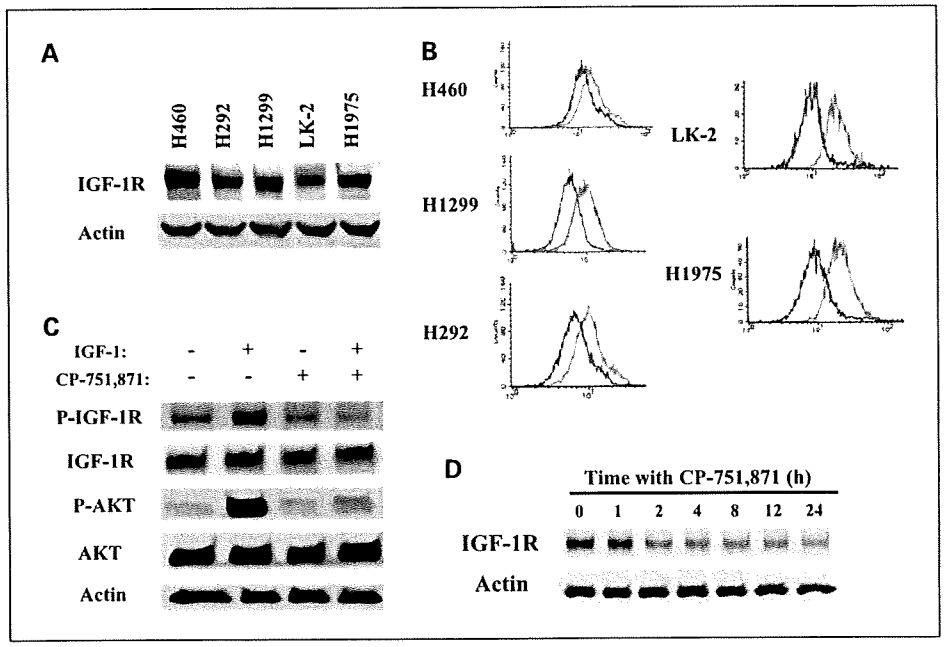

Fig. 1. IGF-1R expression and the effects of CP-751,871 on IGF-IR signaling in human NSCLC cell lines. *A*, H460, H292, H1299, LK-2, and H1975 cells were deprived of serum overnight, lysed, and subjected to immunoblot analysis with antibodies to IGF-IR and to β-actin (loading control). *B*, surface expression of IGF-IR in serum-deprived H460, H1299, H292, LK-2, and H1975 cells was determined by flow cytometry. Representative histograms for cells stained with a mAb to IGF-IR (*green*) or with an isotype-matched control antibody (*black*) are shown. *C*, H460 cells were deprived of serum overnight and then incubated, first in the absence or presence of CP-751,871 (50 nmol/L) for 10 min, and then in the additional absence or presence of IGF-I (50 nmol/L) for 10 min, in serum-free medium. Cell lysates were prepared and subjected to immunoblot analysis with antibodies to phosphorylated (P-) or total forms of IGF-IR or AKT, and to β-actin. *D*, serum-deprived H460 cells were incubated with 50 nmol/L CP-751,871 for the indicated times in serum-free medium, after which cell lysates were subjected to immunoblot analysis with antibodies to IGF-IR and to β-actin.

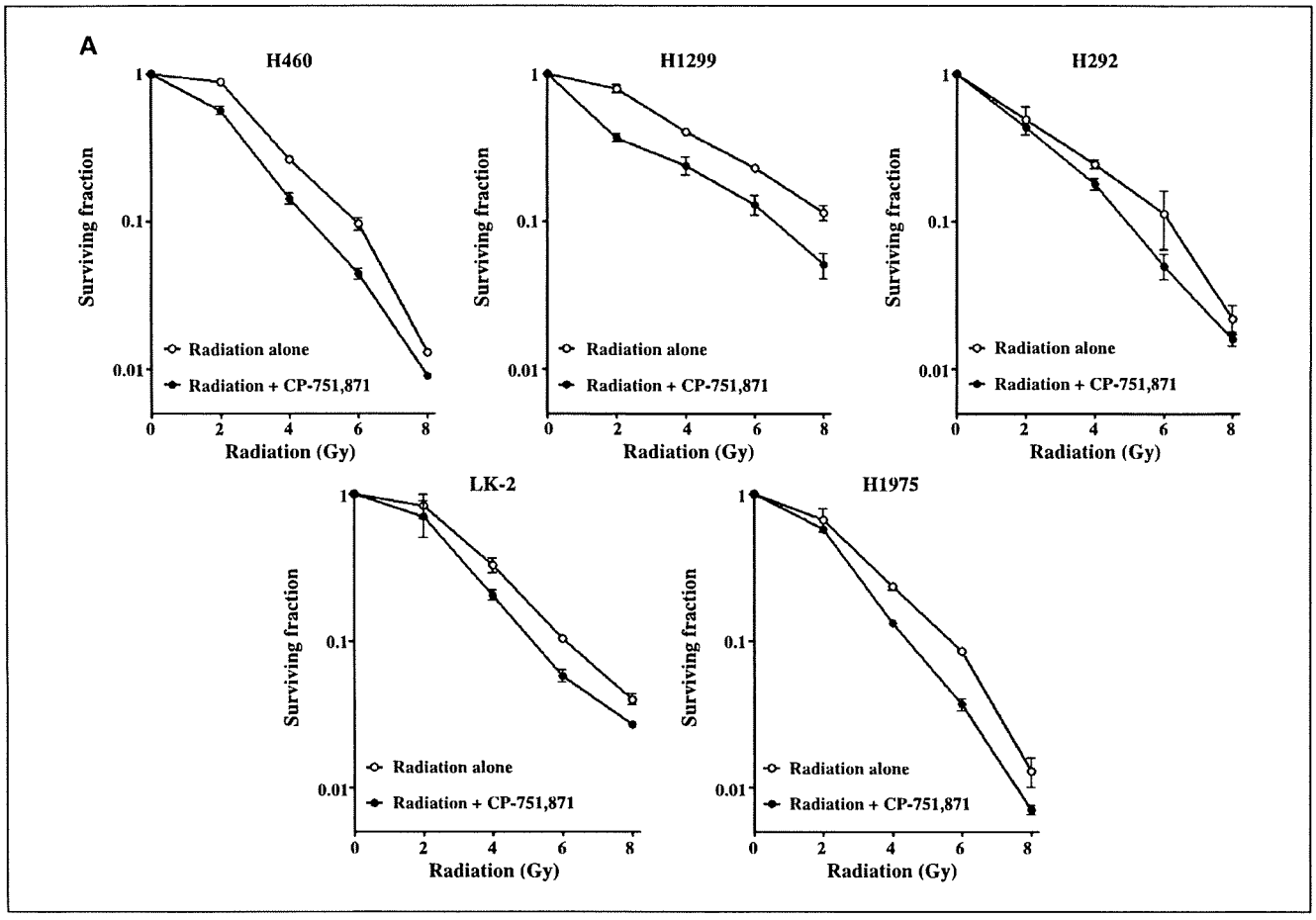

Fig. 2. Effects of CP-751,871 on the sensitivity of NSCLC cells to radiation. *A*, H460, H1299, H292, LK-2, and H1975 cells were deprived of serum overnight, and then exposed to 50 nmol/L CP-751,871 or vehicle (PBS) in serum-free medium before irradiation at the indicated doses. After incubation for 4 h, the cells were washed with PBS and then cultured in antibody-free complete medium for 10 to 14 d for determination of colony-forming ability. Colonies were counted, and the surviving fraction was calculated. Plating efficiency for nonirradiated cells exposed to vehicle or CP-751,871, respectively, was 65.3% and 48.3% for H460 cells, 60.5% and 45.0% for H1299 cells, 63.5% and 52.0% for H292 cells, 31.0% and 27.8% for LK-2 cells, and 87.5% and 52.0% for H1975 cells. All surviving fractions for cells exposed to radiation were corrected for these baseline plating efficiencies. Data, means ± SD from three independent experiments.

8 Gy in all tested cell lines (Fig. 2B), with combination index values ranging between 0.42 and 0.99. These results thus indicated that CP-751,871 increased the radiosensitivity of NSCLC cell lines *in vitro*.

CP-751,871 blocks radiation-induced IGF-IR activation. Activation of IGF-IR plays an important role in preventing the induction of cell death by a variety of stimuli, including ionizing radiation (23). We examined the effects of radiation and CP-751,871 on IGF-IR signaling in NSCLC cells by immunoblot analysis. Radiation induced time-dependent increases in the phosphorylation of IGF-IR and AKT, with these effects being first apparent 2 hours after irradiation and still evident at 8 hours (Fig. 3A). CP-751,871 completely blocked these effects of radiation on IGF-IR and AKT phosphorylation (Fig. 3B), suggesting that radiation-induced activation of IGF-IR in NSCLC cells was inhibited by CP-751,871.

Enhancement of radiation-induced apoptosis by CP-751,871. We next examined whether the inhibitory effect of CP-751,871 on IGF-IR–mediated survival signaling results in enhancement of the proapoptotic activity of radiation. H460 cells were exposed to radiation in the absence or presence of CP-751,871, incubated for 4 h, and then cultured in antibody-free medium for up to a total of 24, 48, or 72 hours. The percentage of apoptotic cells at 72 hours was markedly greater for cells exposed to radiation and CP-751,871 than the sum of the values for cells exposed to radiation or CP-751,871 alone (Fig. 4A). To examine further the effect of radiation and CP-751,871 on the apoptotic pathway, we measured the activity of caspase-3 in cell lysates. Again, combined treatment of H460 cells with CP-751,871 and radiation induced an increase in caspase-3 activity greater than that induced by either treatment alone (Fig. 4B). These data thus indicated that CP-751,871 promoted radiation-induced apoptosis in NSCLC cells.

CP-751,871 inhibits DNA repair in irradiated NSCLC cells. Defects in DNA repair have been associated with enhanced sensitivity of cells to radiation (24), and activated IGF-IR promotes genomic stability by enhancing DNA repair (25). We therefore next investigated the effect of CP-751,871 on DNA repair by immunostaining of cells with antibodies to the phosphorylated form (γ-H2AX) of histone 2AX, foci of which

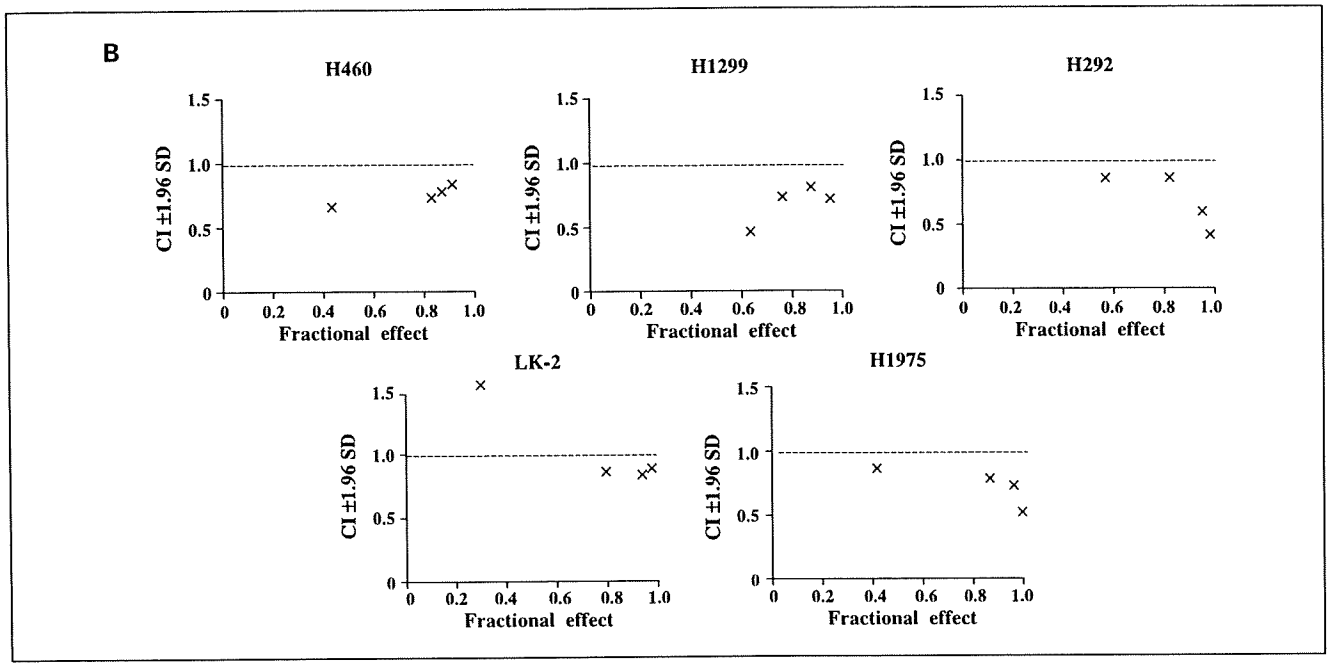

Fig. 2 *Continued.* *B*, Combination index (CI) plots for CP-751,871 plus radiation. Data represent the algebraic estimate of the CI (±1.96 SD) for 50 nmol/L CP-751,871, and radiation doses of 2, 4, 6, and 8 Gy, and correspond to the results shown in *A*. A CI of 1 denotes an additive interaction, of >1 denotes antagonism, and of <1 denotes synergy.

form at DNA double-strand breaks. Irradiation of H460 cells induced the formation of γ-H2AX foci, with the number of such foci being maximal at ~1 hour and having largely returned to the basal level by 24 hours (Fig. 5A). In the presence of CP-751,871, however, the radiation-induced increase in the number of γ-H2AX foci persisted for at least 24 hours. Evaluation of the percentage of H460 cells with γ-H2AX foci at 24 hours after irradiation revealed that CP-751,871 significantly inhibited the repair of double-strand breaks (Fig. 5B). The formation of γ-H2AX foci has been proposed to result in the recruitment of downstream DNA repair factors to the sites of DNA damage (26). The repair protein Rad51 is a key player in homologous recombination during DNA repair (27). Radiation induced the formation of Rad51 foci in H460 cells, with this effect being maximal at 6 hours and still apparent at 24 hours after irradiation (Fig. 5A and C). The radiation-induced formation of Rad51 foci was largely prevented in the presence of CP-751,871. These results thus suggested that CP-751,871 sensitizes NSCLC cells to radiation by inhibiting the Rad51-dependent repair of radiation-induced double-strand breaks.

CP-751,871 enhances radiation-induced tumor regression. To determine whether the CP-751,871–induced radiosensitization of NSCLC cells observed *in vitro* might also be apparent *in vivo*, we implanted H460 or H1299 cells into nude mice to elicit the formation of solid tumors. After tumor formation, the mice were treated with CP-751,871, radiation, or both modalities. Combined treatment with radiation and CP-751,871 inhibited H460 and H1299 tumor growth to a markedly greater extent than did either modality alone (Fig. 6). The tumor growth delays induced by treatment with radiation alone, CP-751,871 alone, or both CP-751,871 and radiation were 13.3, 5.4, and 23.7 days, respectively, for H460 cells; and 1.6, 1.6, and 8.6 days, respectively, for H1299 cells. The enhancement factor for the effect of CP-751,871 on the efficacy of radiation was 1.4 for H460 cells and 4.4 for H1299 cells, revealing the effect to be greater than additive. No pronounced tissue damage or toxicity, such as weight loss, was observed in mice in any of the treatment groups.

Finally, we evaluated whether the combination of CP-751,871 and fractionated radiation treatment would result in inhibition of tumor growth similar to that observed with CP-751,871 plus single-fraction radiation. We examined only the H460 xenograft model in the fractionated radiotherapy experiments. The tumor growth delays induced by treatment with radiation alone, CP-751,871 alone, or both CP-751,871 and radiation were 6.4, 2.7, and 27.2 days, respectively (Supplementary Fig. S1). The enhancement factor for the effect of CP-751,871 on the efficacy of radiation was 3.8. Again, there was no evidence of toxicity, such as body weight loss, and there were no animal deaths in any of the four groups. These data suggested that CP-751,871 enhances the tumor response to both single-dose and fractionated radiotherapy *in vivo*.

Discussion

Several mAbs to IGF-IR that block ligand binding and induce receptor down-regulation have been developed (8, 9). We have now shown that CP-751,871 suppresses IGF-IR signaling through direct antagonism of ligand binding and receptor down-regulation. We also found that CP-751,871 sensitizes tumor cells to radiation *in vitro*, and that combination treatment with CP-751,871 and radiation results in a greater-than-additive delay in tumor growth in tumor xenograft models without systemic toxicity. The mechanism by which CP-751,871 enhances radiosensitivity seems to involve inhibition of the repair

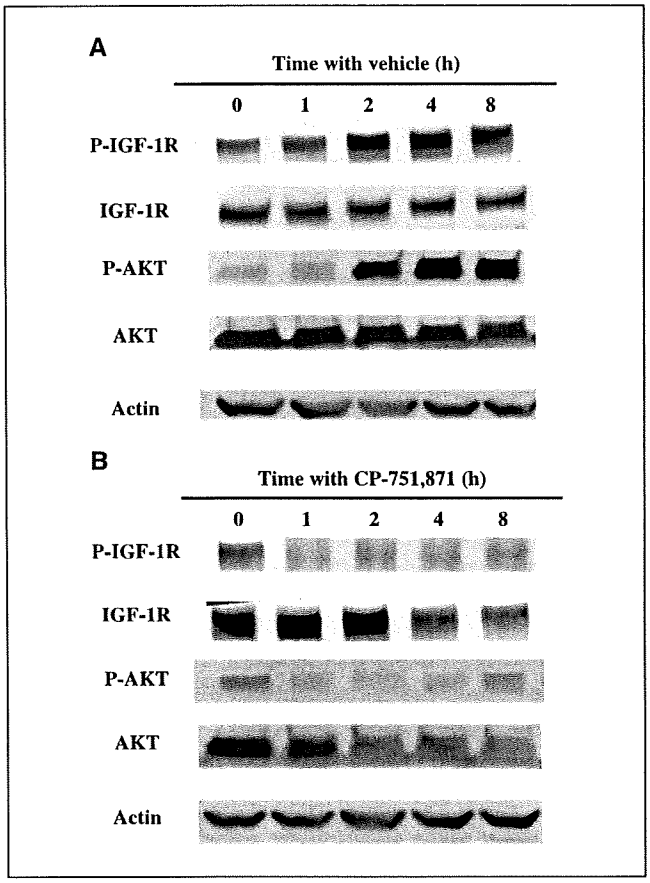

Fig. 3. Effects of CP-751,871 on IGF-IR and AKT phosphorylation induced by radiation. Serum-deprived H460 cells were exposed to 10 Gy of radiation in the absence (*A*) or presence (*B*) of 50 nmol/L CP-751,871 in serum-free medium. Cell lysates were prepared at the indicated times after irradiation and subjected to immunoblot analysis with antibodies to phosphorylated or total forms of IGF-IR or AKT, and to β-actin.

of radiation-induced double-strand breaks and potentiation of cancer cell apoptosis.

Cellular stress induced by several chemotherapeutic agents or radiation triggers the activation of IGF-IR signaling (14, 28, 29). We found that radiation induced IGF-IR phosphorylation in NSCLC cells. Other growth factor receptors, such as the epidermal growth factor receptor, are also activated by radiation (30, 31). Reactive oxygen species and reactive nitrogen species generated by radiation are thought to shift the steady-state tyrosine phosphorylation status of epidermal growth factor receptor to the phosphorylated (active) form as a result of the inactivation of critical cysteine residues in the catalytic center of corresponding protein phosphatases (32–34). Activated epidermal growth factor receptor signaling in turn promotes the release of paracrine ligands, such as the pro form of transforming growth factor α, and the consequent activation of receptors and intracellular signaling pathways (35). The insulin receptor is a receptor tyrosine kinase that is also activated by a reactive oxygen species–dependent mechanism (30, 36). Although the precise mechanism by which radiation induces IGF-IR phosphorylation remains to be elucidated, these previous observations suggest that radiation-induced IGF-IR activation may occur in ligand-dependent or ligand-independent manners. We found that CP-751,871 blocked radiation-induced IGF-IR activation, likely as a result of both competition with ligand for binding to IGF-IR and receptor down-regulation. Given that radiation-induced IGF-IR phosphorylation contributes to radiation-induced acceleration of tumor cell repopulation and enhancement of radioresistance (37), our data indicate that CP-751,871 increases radiosensitivity by suppressing radiation-induced IGF-IR activation.

IGF-IR activation results in suppression of apoptosis signaling pathways and promotion of cell survival. Previous studies have shown that another type of antibody to IGF-IR promotes apoptotic cell death (8, 38). In the present study, we found that the combination of CP-751,871 and radiation induced NSCLC cell apoptosis as well as the activation of caspase-3 to an extent greater than that apparent with either agent alone. Our data thus suggest that CP-751,871 inhibits antiapoptotic signaling elicited by radiation-induced IGF-IR activation. However, the fraction of apoptotic cells detected under our experimental conditions was relatively small. Given that the relation between apoptosis and radiosensitivity is controversial (39–41), we examined additional mechanisms by which CP-751,871 might contribute to radiosensitization.

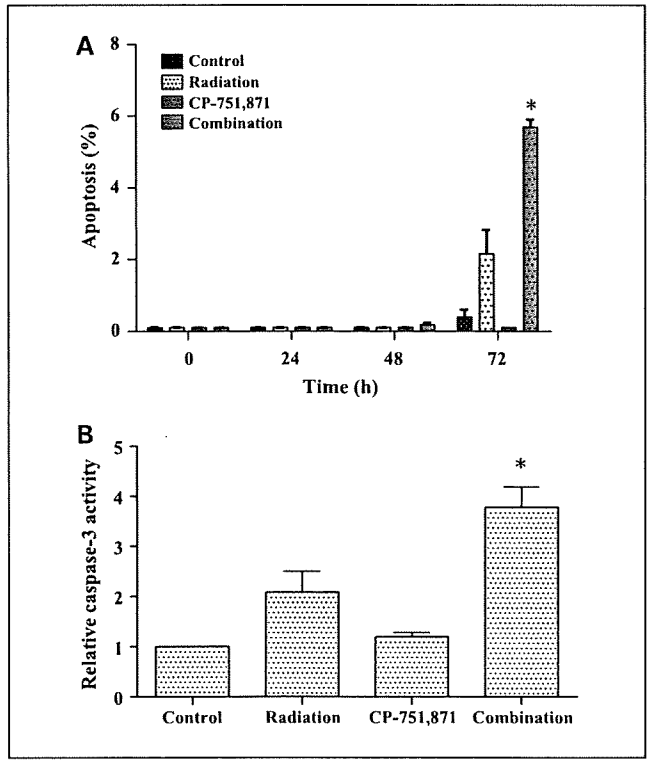

Fig. 4. Effects of CP-751,871 on radiation-induced apoptosis and caspase-3 activity in H460 cells. *A*, serum-deprived H460 cells were exposed (or not) to 10 Gy of radiation in the presence of 50 nmol/L CP-751,871 or vehicle (PBS) in serum-free medium, incubated for 4 h, and then cultured in antibody-free complete medium for up to a total of 24, 48, or 72 h. The percentage of apoptotic cells was then determined by terminal deoxyribonucleotide transferase–mediated nick-end labeling staining. *B*, lysates of cells treated as in *A* were assayed for caspase-3 activity 72 h after irradiation. Data, means ± SD from three independent experiments; those in *B* are expressed relative to the corresponding value for the control condition. *, $P < 0.01$ versus the corresponding value for treatment with radiation or CP-751,871 alone.

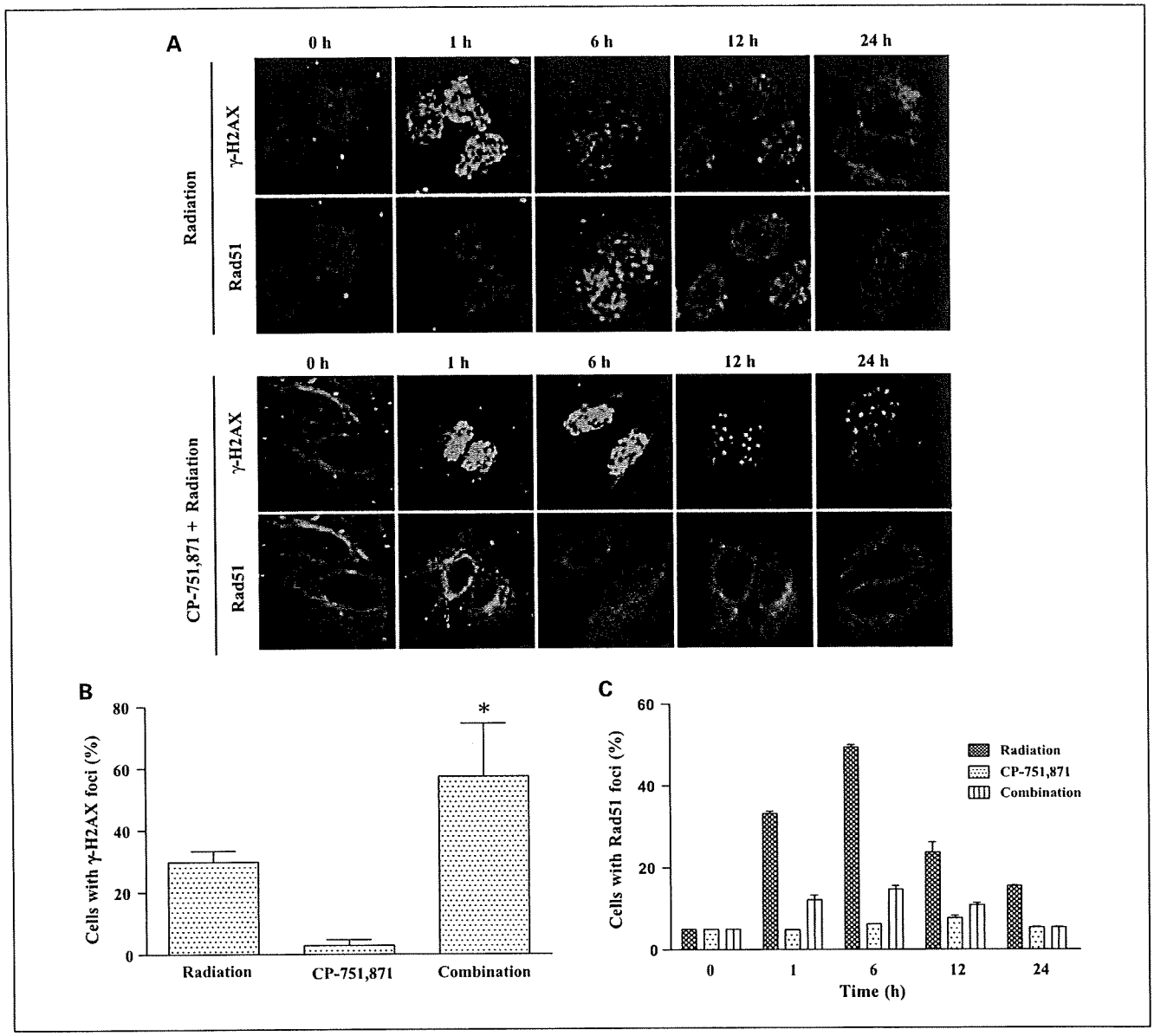

Fig. 5. Effects of CP-751,871 on the radiation-induced formation of γ-H2AX and Rad51 foci in H460 cells. *A*, serum-deprived cells were exposed to 10 Gy of radiation in the presence of vehicle (PBS) or 50 nmol/L CP-751,871 in serum-free-medium, incubated for 4 h, and then cultured for up to the indicated total times in antibody-free complete medium. The cells were then fixed and subjected to immunofluorescence staining for γ-H2AX (*green fluorescence*) and Rad51 (*red fluorescence*). *B*, cells treated as in *A* were fixed at 24 h after irradiation, and the percentage of cells containing γ-H2AX foci was determined. Data, means ± SD from three independent experiments. *, $P < 0.05$ versus the corresponding value for cells exposed to radiation or CP-751,871 alone. *C*, cells treated as in *A* were evaluated for the percentage of cells containing Rad51 foci. Data, means ± SD from three independent experiments.

The IGF-IR signaling pathway has been implicated in regulation of DNA repair (29, 42, 43). We investigated the effects of CP-751,871 on the repair of radiation-induced DNA damage by immunofluorescence staining of γ-H2AX. Given that γ-H2AX appears rapidly at DNA double-strand breaks and disappears as repair proceeds (44), it serves as a sensitive and specific marker for unrepaired DNA damage. We found that CP-751,871 inhibited the repair of radiation-induced double-strand breaks. Ligand-induced IGF-IR activation was previously shown to attenuate a cytosolic interaction between the DNA repair protein Rad51 and insulin receptor substrate 1, a key mediator of IGF-IR signaling, resulting in the translocation of Rad51 to the sites of DNA double-strand breaks (43). Given that radiation induced IGF-IR activation, we examined whether CP-751,871 in combination with radiation might affect the subcellular distribution of Rad51. We found that radiation increased the number of nuclear Rad51 foci, likely as a result of radiation-induced IGF-IR activation, whereas CP-751,871 inhibited this effect. These results indicate that prevention of radiation-induced IGF-IR activation by

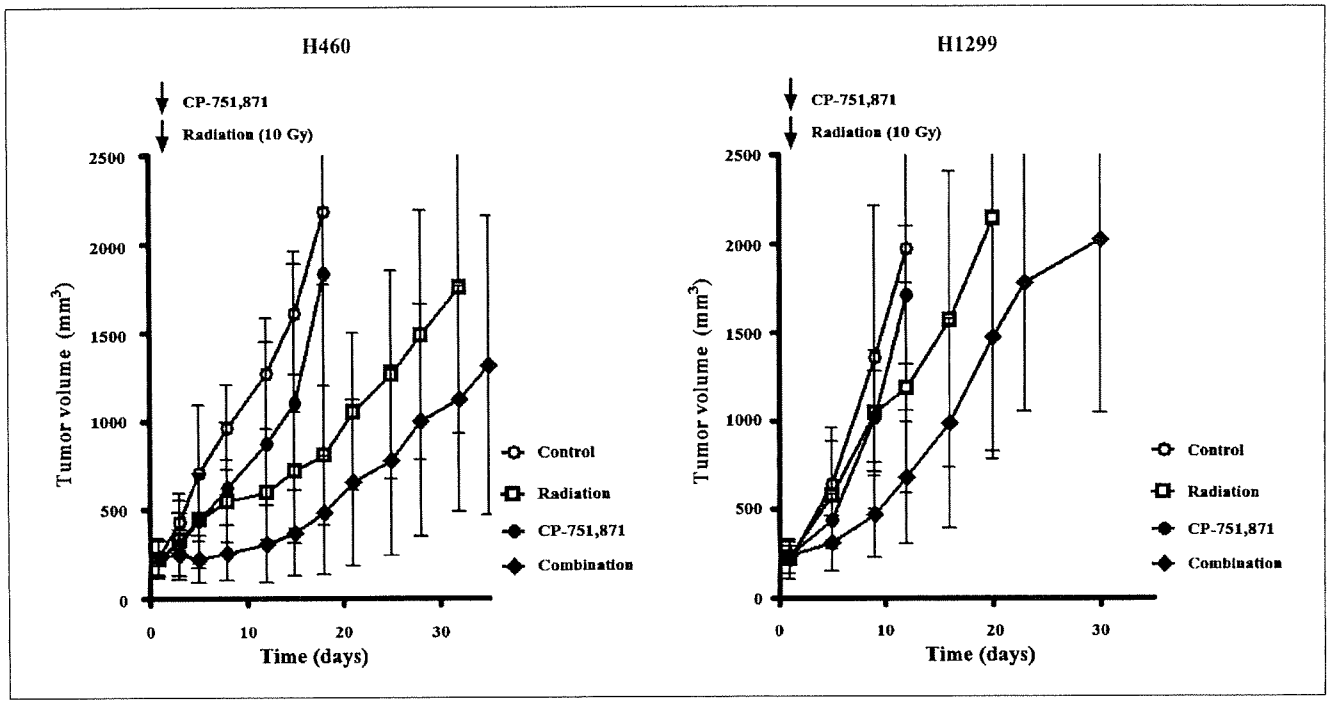

Fig. 6. Effects of CP-751,871 on the growth of H460 or H1299 tumors in mice subjected to single-dose radiotherapy. H460 or H1299 cells were implanted into the right hind limb of nude mice and allowed to form tumors with an average volume of ~200 to 250 mm^3. The mice were divided into four treatment groups: control, radiation alone, CP-751,871 alone, or the combination of CP-751,871 and radiation. CP-751,871 (500 μg) or vehicle was given i.p. in a single dose, and mice in the radiation groups were subjected to irradiation with a single dose of 10 Gy on day 1 of drug treatment. Tumor volume was measured at the indicated times after the onset of treatment. Data, means ± SD from five mice per group.

CP-751,871 results in insufficient recruitment of Rad51 to double-strand breaks and consequent impairment of DNA repair. Although it is possible that CP-751,871 also inhibits DNA repair in a manner independent of Rad51, our results suggest that radiosensitization by CP-751,871 is mediated at least in part by suppression of Rad51-dependent DNA repair.

In conclusion, our results indicate that CP-751,871 blocks radiation-induced IGF-IR activation, and consequently sensitizes tumor cells to radiation by inhibiting DNA repair and promoting apoptosis. Our preclinical data suggest that clinical evaluation of CP-751,871 in combination with radiation as a potential anticancer therapy is warranted.

Disclosure of Potential Conflicts of Interest

No potential conflicts of interest were disclosed.

Acknowledgments

We thank Shoko Ono for technical assistance.

References

1. Sell C, Rubini M, Rubin R, Liu JP, Efstratiadis A, Baserga R. Simian virus 40 large tumor antigen is unable to transform mouse embryonic fibroblasts lacking type 1 insulin-like growth factor receptor. Proc Natl Acad Sci U S A 1993;90:11217–21.
2. O'Connor R, Kauffmann-Zeh A, Liu Y, et al. Identification of domains of the insulin-like growth factor I receptor that are required for protection from apoptosis. Mol Cell Biol 1997;17:427–35.
3. Pietrzkowski Z, Mulholland G, Gomella L, Jameson BA, Wernicke D, Baserga R. Inhibition of growth of prostatic cancer cell lines by peptide analogues of insulin-like growth factor 1. Cancer Res 1993;53:1102–6.
4. D'Ambrosio C, Ferber A, Resnicoff M, Baserga R. A soluble insulin-like growth factor I receptor that induces apoptosis of tumor cells *in vivo* and inhibits tumorigenesis. Cancer Res 1996;56:4013–20.
5. Muller M, Dietel M, Turzynski A, Wiechen K. Antisense phosphorothioate oligodeoxynucleotide down-regulation of the insulin-like growth factor I receptor in ovarian cancer cells. Int J Cancer 1998;77:567–71.
6. Scotlandi K, Avnet S, Benini S, et al. Expression of an IGF-I receptor dominant negative mutant induces apoptosis, inhibits tumorigenesis and enhances chemosensitivity in Ewing's sarcoma cells. Int J Cancer 2002;101:11–6.
7. Garcia-Echeverria C, Pearson MA, Marti A, et al. *In vivo* antitumor activity of NVP-AEW541-a novel, potent, and selective inhibitor of the IGF-IR kinase. Cancer Cell 2004;5:231–9.
8. Maloney EK, McLaughlin JL, Dagdigian NE, et al. An anti-insulin-like growth factor I receptor antibody that is a potent inhibitor of cancer cell proliferation. Cancer Res 2003;63:5073–83.
9. Burtrum D, Zhu Z, Lu D, et al. A fully human monoclonal antibody to the insulin-like growth factor I receptor blocks ligand-dependent signaling and inhibits human tumor growth *in vivo*. Cancer Res 2003;63:8912–21.
10. Cohen BD, Baker DA, Soderstrom C, et al. Combination therapy enhances the inhibition of tumor growth with the fully human anti-type 1 insulin-like growth factor receptor monoclonal antibody CP-751,871. Clin Cancer Res 2005;11:2063–73.
11. Wang Y, Hailey J, Williams D, et al. Inhibition of insulin-like growth factor-I receptor (IGF-IR) signaling and tumor cell growth by a fully human neutralizing anti-IGF-IR antibody. Mol Cancer Ther 2005;4:1214–21.
12. Sachdev D, Yee D. Disrupting insulin-like growth factor signaling as a potential cancer therapy. Mol Cancer Ther 2007;6:1–12.
13. Garber K. IGF-1: old growth factor shines as new drug target. J Natl Cancer Inst 2005;97:790–2.
14. Turner BC, Haffty BG, Narayanan L, et al.

Insulin-like growth factor-I receptor overexpression mediates cellular radioresistance and local breast cancer recurrence after lumpectomy and radiation. Cancer Res 1997;57:3079–83.

15. Rocha RL, Hilsenbeck SG, Jackson JG, et al. Insulin-like growth factor binding protein-3 and insulin receptor substrate-1 in breast cancer: correlation with clinical parameters and disease-free survival. Clin Cancer Res 1997;3:103–9.
16. Kuhn C, Hurwitz SA, Kumar MG, Cotton J, Spandau DF. Activation of the insulin-like growth factor-1 receptor promotes the survival of human keratinocytes following ultraviolet B irradiation. Int J Cancer 1999;80:431–8.
17. Wen B, Deutsch E, Marangoni E, et al. Tyrphostin AG 1024 modulates radiosensitivity in human breast cancer cells. Br J Cancer 2001; 85:2017–21.
18. Cosaceanu D, Carapancea M, Castro J, et al. Modulation of response to radiation of human lung cancer cells following insulin-like growth factor 1 receptor inactivation. Cancer Lett 2005;222:173–81.
19. Sak A, Stueben G, Groneberg M, Bocker W, Stuschke M. Targeting of Rad51-dependent homologous recombination: implications for the radiation sensitivity of human lung cancer cell lines. Br J Cancer 2005;92:1089–97.
20. Albert JM, Cao C, Kim KW, et al. Inhibition of poly(ADP-ribose) polymerase enhances cell death and improves tumor growth delay in irradiated lung cancer models. Clin Cancer Res 2007;13:3033–42.
21. United Kingdom Co-ordinating Committee on Cancer Research. Guidelines for the welfare of animals in experimental neoplasia (2nd ed.). Br J Cancer 1998;77:1–10.
22. Chou TC, Talalay P. Quantitative analysis of dose-effect relationships: the combined effects of multiple drugs or enzyme inhibitors. Adv Enzyme Regul 1984;22:27–55.
23. Tezuka M, Watanabe H, Nakamura S, et al. Antiapoptotic activity is dispensable for insulin-like growth factor I receptor-mediated clonogenic radioresistance after γ-irradiation. Clin Cancer Res 2001;7:3206–14.
24. Gao Y, Ferguson DO, Xie W, et al. Interplay of p53 and DNA-repair protein XRCC4 in tumorigenesis, genomic stability and development. Nature 2000;404:897–900.
25. Yang S, Chintapalli J, Sodagum L, et al. Activated IGF-1R inhibits hyperglycemia-induced DNA damage and promotes DNA repair by homologous recombination. Am J Physiol Renal Physiol 2005;289:F1144–52.
26. Burma S, Chen BP, Murphy M, Kurimasa A, Chen DJ. ATM phosphorylates histone H2AX in response to DNA double-strand breaks. J Biol Chem 2001;276:42462–7.
27. Chen G, Yuan SS, Liu W, et al. Radiation-induced assembly of Rad51 and Rad52 recombination complex requires ATM and c-Abl. J Biol Chem 1999;274:12748–52.
28. Gooch JL, Van Den Berg CL, Yee D. Insulin-like growth factor (IGF)-I rescues breast cancer cells from chemotherapy-induced cell death-proliferative and anti-apoptotic effects. Breast Cancer Res Treat 1999;56:1–10.
29. Cosaceanu D, Budiu RA, Carapancea M, Castro J, Lewensohn R, Dricu A. Ionizing radiation activates IGF-1R triggering a cytoprotective signaling by interfering with Ku-DNA binding and by modulating Ku86 expression via a p38 kinase-dependent mechanism. Oncogene 2007;26:2423–34.
30. Bowers G, Reardon D, Hewitt T, et al. The relative role of ErbB1-4 receptor tyrosine kinases in radiation signal transduction responses of human carcinoma cells. Oncogene 2001;20:1388–97.
31. Griffin RJ, Williams BW, Wild R, Cherrington JM, Park H, Song CW. Simultaneous inhibition of the receptor kinase activity of vascular endothelial, fibroblast, and platelet-derived growth factors suppresses tumor growth and enhances tumor radiation response. Cancer Res 2002;62:1702–6.
32. Schmidt-Ullrich RK, Dent P, Grant S, Mikkelsen RB, Valerie K. Signal transduction and cellular radiation responses. Radiat Res 2000;153: 245–57.
33. Leach JK, Van Tuyle G, Lin PS, Schmidt-Ullrich R, Mikkelsen RB. Ionizing radiation-induced, mitochondria-dependent generation of reactive oxygen/nitrogen. Cancer Res 2001;61: 3894–901.
34. Leach JK, Black SM, Schmidt-Ullrich RK, Mikkelsen RB. Activation of constitutive nitric-oxide synthase activity is an early signaling event induced by ionizing radiation. J Biol Chem 2002;277:15400–6.
35. Shvartsman SY, Hagan MP, Yacoub A, Dent P, Wiley HS, Lauffenburger DA. Autocrine loops with positive feedback enable context-dependent cell signaling. Am J Physiol Cell Physiol 2002;282: C545–59.
36. Dent P, Han SI, Mitchell C, et al. Inhibition of insulin/IGF-1 receptor signaling enhances bile acid toxicity in primary hepatocytes. Biochem Pharmacol 2005;70:1685–96.
37. Dent P, Yacoub A, Contessa J, et al. Stress and radiation-induced activation of multiple intracellular signaling pathways. Radiat Res 2003;159: 283–300.
38. Benini S, Manara MC, Baldini N, et al. Inhibition of insulin-like growth factor I receptor increases the antitumor activity of doxorubicin and vincristine against Ewing's sarcoma cells. Clin Cancer Res 2001;7:1790–7.
39. Akagi Y, Ito K, Sawada S. Radiation-induced apoptosis and necrosis in Molt-4 cells: a study of dose-effect relationships and their modification. Int J Radiat Biol 1993;64: 47–56.
40. Lawrence TS, Davis MA, Hough A, Rehemtulla A. The role of apoptosis in 2',2'-difluoro-2'-deoxycytidine (gemcitabine)-mediated radiosensitization. Clin Cancer Res 2001;7:314–9.
41. Pawlik TM, Keyomarsi K. Role of cell cycle in mediating sensitivity to radiotherapy. Int J Radiat Oncol Biol Phys 2004;59:928–42.
42. Heron-Milhavet L, LeRoith D. Insulin-like growth factor I induces MDM2-dependent degradation of p53 via the p38 MAPK pathway in response to DNA damage. J Biol Chem 2002;277: 15600–6.
43. Trojanek J, Ho T, Del Valle L, et al. Role of the insulin-like growth factor I/insulin receptor substrate 1 axis in Rad51 trafficking and DNA repair by homologous recombination. Mol Cell Biol 2003;23:7510–24.
44. Rogakou EP, Pilch DR, Orr AH, Ivanova VS, Bonner WM. DNA double-stranded breaks induce histone H2AX phosphorylation on serine 139. J Biol Chem 1998;273:5858–68.

Tumor and Stem Cell Biology

Cancer Research

FOXQ1 Is Overexpressed in Colorectal Cancer and Enhances Tumorigenicity and Tumor Growth

Hiroyasu Kaneda[1,2], Tokuzo Arao[1], Kaoru Tanaka[1,2], Daisuke Tamura[1], Keiichi Aomatsu[1], Kanae Kudo[1], Kazuko Sakai[1], Marco A. De Velasco[1], Kazuko Matsumoto[1], Yoshihiko Fujita[1], Yasuhide Yamada[3], Junji Tsurutani[2], Isamu Okamoto[2], Kazuhiko Nakagawa[2], and Kazuto Nishio[1]

Abstract

Forkhead box Q1 (FOXQ1) is a member of the forkhead transcription factor family, and it has recently been proposed to participate in gastric acid secretion and mucin gene expression in mice. However, the role of FOXQ1 in humans and especially in cancer cells remains unknown. We found that *FOXQ1* mRNA is overexpressed in clinical specimens of colorectal cancer (CRC; 28-fold/colonic mucosa). A microarray analysis revealed that the knockdown of *FOXQ1* using small interfering RNA resulted in a decrease in $p21^{CIP1/WAF1}$ expression, and a reporter assay and a chromatin immunoprecipitation assay showed that *p21* was one of the target genes of FOXQ1. Stable FOXQ1-overexpressing cells (H1299/FOXQ1) exhibited elevated levels of p21 expression and inhibition of apoptosis induced by doxorubicin or camptothecin. Although cellular proliferation was decreased in H1299/FOXQ1 cells *in vitro*, H1299/FOXQ1 cells significantly increased tumorigenicity [enhanced green fluorescent protein (EGFP): 2/15, FOXQ1: 7/15] and enhanced tumor growth (437 ± 301 versus 1735 ± 769 mm^3, $P < 0.001$) *in vivo*. Meanwhile, stable p21 knockdown of H1299/FOXQ1 cells increased tumor growth, suggesting that FOXQ1 promotes tumor growth independent of p21. Microarray analysis of H1299/EGFP and H1299/FOXQ1 revealed that FOXQ1 overexpression upregulated several genes that have positive roles for tumor growth, including *VEGFA, WNT3A, RSPO2,* and *BCL11A*. CD31 and terminal deoxynucleotidyl transferase-mediated dUTP nick end labeling staining of the tumor specimens showed that FOXQ1 overexpression mediated the angiogenic and antiapoptotic effect *in vivo*. In conclusion, FOXQ1 is overexpressed in CRC and enhances tumorigenicity and tumor growth presumably through its angiogenic and antiapoptotic effects. Our findings show that FOXQ1 is a new member of the cancer-related FOX family. *Cancer Res; 70(5); 2053–63. ©2010 AACR.*

Introduction

The forkhead box (*Fox*) gene family is a large and diverse group of transcription factors that share certain characteristics of a conserved, ~100 amino acid DNA-binding motif known as the forkhead or winged helix domain; over 100 proteins with forkhead domains have been identified, comprising at least 17 subclasses to date (1). The Fox gene family plays various important roles, not only in biological processes including development, metabolism, immunology, and senescence but also in cancer development (2, 3).

Forkhead box Q1 (*FOXQ1*, also known as HFH1) is a member of the FOX gene family and contains the core DNA binding domain, whereas the flanking wings of FOXQ1 contribute to its sequence specificity (4). As a transcription factor, FOXQ1 is known to repress the promoter activity of smooth muscle–specific genes, such as telokin and SM22α, in A10 vascular muscle cells (5), and FOXQ1 expression is regulated by Hoxa1 in embryonic stem cells (6). The biological function of *Foxq1* has been clearly identified in hair follicle differentiation in satin (sa) homozygous mice (7); interestingly, satin mice also exhibit suppressed natural killer cell function and T-cell function, suggesting a relation with immunology. Satin mice have provided evidence that Hoxc13 regulates foxq1 expression and that "cross-talk" occurs between Homeobox and Fox (8). Foxq1 mRNA is widely expressed in murine tissues, with particularly high expression levels in the stomach and bladder (5). Recently, two important findings have been reported regarding its involvement in stomach surface cells. Foxq1-deficient mice exhibit a lack of gastric acid secretion in response to various secretagogue stimuli (9). On the other hand, Foxq1 regulates gastric MUC5AC synthesis, providing clues as to the lineage-specific cell differentiation in gastric surface epithelia (10). Despite accumulating evidence supporting the biological function of the murine foxq1 gene in hair follicle

Authors' Affiliations: Departments of [1]Genome Biology and [2]Medical Oncology, Kinki University School of Medicine, Osaka-Sayama, Osaka, Japan and [3]Department of Medical Oncology, National Cancer Center Hospital, Chuo-ku, Tokyo, Japan

Note: Supplementary data for this article are available at Cancer Research Online (http://cancerres.aacrjournals.org/).

Corresponding Author: Kazuto Nishio, Department of Genome Biology, Kinki University School of Medicine, 377-2 Ohno-higashi, Osaka-Sayama, Osaka 589-8511, Japan. Phone: 81-72-366-0221; Fax: 81-72-366-0206; E-mail: knishio@med.kindai.ac.jp.

doi: 10.1158/0008-5472.CAN-09-2161

morphogenesis and gastric epithelial cells, no data regarding the cellular and biological functions of human *FOXQ1*, especially in cancer cells, are available.

$p21^{CIP1/WAF1}$ (hereafter called p21) is a member of the cip/kip family of cyclin kinase inhibitors, and initial reports have shown that p21 functions as a G_1 cyclin kinase inhibitor (11, 12) and a downstream molecule of p53 (13). p21 possesses a variety of cellular functions, including the negative modulation of cell cycle progression (14), cellular differentiation (15), and the regulation of p53-dependent antiapoptosis (reviewed in ref. 16). The expression of p21 is regulated by both p53-dependent and p53-independent mechanisms at the transcriptional level. Other regulatory mechanisms of p21 expression involve proteasome-mediated degradation, mRNA stability, alterations in the epigenetic silencing of the p21 promoter, and secondary decreases resulting from viral activity targeting p53, such as the activities of human papilloma virus and hepatitis C virus (17). However, its expression is considered to be regulated mainly at the transcriptional level (18). Accumulating data indicate that many molecules from diverse signaling pathways can activate or repress the p21 promoter, including p53, transforming growth factor-β (TGF-β), c-jun, Myc, Sp1/Sp3, signal transducers and activators of transcriptions, CAAT/enhancer binding protein-α (C/EBP-α), C/EBP-β, basic helix-loop-helix proteins, and myogenic differentiation 1 (reviewed in ref. 19). Thus, p21 is integrally involved in both cell cycle and apoptosis; therefore, identifying its regulatory molecules is of great importance.

We performed a microarray analysis of clinical samples of paired colorectal cancer (CRC) specimens and normal colonic mucosa specimens to identify genes that were overexpressed in CRC. Our results revealed that *FOXQ1* gene expression was ~28-fold higher in CRC than in normal colonic mucosa, and we hypothesized that FOXQ1 may play a role in CRC. In the present study, we investigated the biological function of FOXQ1.

Materials and Methods

Antibodies. The following antibodies were used: anti-p21, anti-p53, anti-cdk2, anti-cdk4, anti-cyclin D, anti-phosphorylated Rb, anti-poly(ADP-ribose) polymerase (PARP), anti-cleaved PARP, anti-caspase-3, anti-cleaved caspase-3, secondary antibodies, and Myc-tag mouse antibody (Cell Signaling), as well as anti-β-actin (Santa Cruz Biotechnology). A mouse anti-CD31 monoclonal antibody was purchased from BD Biosciences.

Cell lines and cultures. The DLD-1, MKN74, H1299, SBC3, and U251 cell lines were cultured in RPMI 1640 (Sigma). The WiDr, CoLo320DM, and human embryonic kidney cell line 293 (HEK293) cell lines were cultured in DMEM (Sigma), and the LoVo cell line was cultured in Ham/F12 medium [Life Technologies Bethesda Research Laboratories (BRL)]. All media were supplemented with 10% heat-inactivated fetal bovine serum (Life Technologies BRL), and the cell lines were maintained in a 5% CO_2-humidified atmosphere at 37°C.

Patients and samples. Paired CRC and noncancerous colonic mucosa samples were evaluated using a microarray analysis in the first consecutive 10 patients. These samples and another 36 CRC samples were analyzed using real-time reverse transcription–PCR (RT-PCR). The RNA extraction method and the quality check protocol have been previously described (20). This study was approved by the institutional review board of the National Cancer Center Hospital, and written informed consent was obtained from all the patients.

Plasmid construction, viral production, and stable transfectants. The cDNA fragment encoding human full-length FOXQ1 was isolated using PCR and Prime STAR HS DNA polymerase (TaKaRa) with 5′-GGG AAT TCG CGG CCA TGA AGT TGG AGG TCT TCG TC-3′ and 5′-CCC TCG AGC GCT ACT CAG GCT AGG AGC GTC TCC AC-3′ sense and antisense primers, respectively. The methods used in this section have been previously described (21). Short hairpin RNA (shRNA) targeting p21 was constructed using oligonucleotides encoding small interfering RNA (siRNA) directed against p21 and a nonspecific target as follows: 5′-CTA AGA GTG CTG GGC ATT TTT-3′ for p21 shRNA and 5′-TGT TCG CAG TAC GGT AAT GTT-3′ for control shRNA. They were cloned into an RNAi-Ready pSIREN-RetroQZsGreen vector (Clontech) according to manufacturer's protocol. The stable transfectants expressing enhanced green fluorescent protein (EGFP) or FOXQ1 or FOXQ1 with shRNA targeting p21 for each cell line were designated as HEK293/EGFP, HEK293/FOXQ1, CoLo320/EGFP, CoLo320/FOXQ1, H1299/EGFP, H1299/FOXQ1, H1299/FOXQ1/sh-control, and H1299/FOXQ1/sh-p21. The FOXQ1 human cDNA was tagged at the NH_2 terminus with the myc epitope using the pCMV-Myc vector (Clontech) for chromatin immunoprecipitation (ChIP) assay.

SiRNA transfection. Two different sequences of siRNA targeting human FOXQ1 and negative control siRNA were purchased from QIAGEN. The sequences of FOXQ1 and control siRNA were as follows: FOXQ1#1 sense, 5′-CCA UCA AAC GUG CCU UAA A-3′ and antisense, 5′-UUU AAG GCA CGU UUG AUG G-3′; FOXQ1#4 sense, 5′-CGC GGA CUU UGC ACU UUG A-3′ and antisense, 5′-UCA AAG UGC AAA GUC CGC G-3′; control siRNA (scramble) sense, 5′-UUC UCC GAA CGU GUC ACG U-3′ and antisense, 5′-ACG UGA CAC GUU CGG AGA A-3′; control siRNA (GFP) sense, 5′-GCA AGC UGA CCC UGA AGU UCA U-3′ and antisense, 5′-GAA CUU CAG GGU CAG CUU GCC G-3′. The methods of transfection have been previously described (22).

Real-time RT-PCR and Western blot analysis. The methods used in this section have been previously described (21). The primers used for real-time RT-PCR were purchased from Takara as follows: FOXQ1 forward, 5′-CGC GGA CTT TGC ACT TTG AA-3′ and reverse, 5′-AGC TTT AAG GCA CGT TTG ATG GAG-3′; p21 forward, 5′-TCC AGC GAC CTT CCT CAT CCA C-3′ and reverse, 5′-TCC ATA GCC TCT ACT GCC ACC ATC-3′; glyceraldehyde-3-phosphate dehydrogenase (GAPD) forward, 5′-GCA CCG TCA AGG CTG AGA AC-3′ and reverse, 5′-ATG GTG GTG AAG ACG CCA GT-3′. The experiment was performed in triplicate.